Interactive comment on Atmos. Chem. Phys. Discuss., https://doi.org/10.5194/acp-2019-582, 2019.

We thank the reviewers for their comments. Below, we present responses, labeled as Rn (n being the number of the response) for easier referencing, to each comment in blue colour.

Response to Anonymous Referee #2

General Comments:
The authors have reported on a series of experiments aimed at quantifying the total and speciated HOM formed from the oxidation of important aromatic VOCs using two different facilities: a flowtube and an environmental chamber. The data analysis is enlightening and a number of useful interpretations are made that will help the field continue to advance understanding of this potentially impactful atmospheric phenomenon. In general though, I found the lack of quantitative conclusions disappointing. The yield estimates provided are somewhat provocative because they are so high compared to previous reported values, but it is unclear how the atmospheric model community should use these estimates, or if they should use them at all. I recommend this manuscript be published, but I have some reservations with the overall messaging.

R1. Both anonymous reviewers made us aware that our statements (in abstract and conclusions) about model implementations of SOA and HOM were unclear and somewhat misleading. We therefore will clarify our intentions here, as they are relevant for several later comments as well.

In this manuscript, we did not aim at parameterisations for atmospheric models. Nor would we have been able to, as only a limited set of atmospheric conditions and oxidation products were sampled in our experiments. Instead, we tried to point out that the yields of both SOA and HOM are likely to be extremely sensitive to variations in the specific conditions, and thus modelers need to carefully consider which atmospheric conditions a certain laboratory study result is applicable. In this work, we show that the OH concentration affects both total HOM yield as well as HOM composition. OH has been a less frequently considered parameter in HOM research so far, but of course is critical in aromatic oxidation. It is clear that more studies are needed to understand complex and coupled processes of aromatic oxidation to be able to properly model it. We think that our quantitative results increase the general understanding of HOM formation from aromatic systems; however, the absolute values are most useful for other experimentalists to interpret and plan their HOM and SOA studies. We have clarified the relevant sentences in the *Abstract* and *Summary and Conclusions* as follows:

Abstract: “Based on our results, we conclude that HOM yield and composition in aromatic systems strongly depend on OH and VOC concentration and more studies are needed to fully understand this effect in formation of HOM and, consequently, SOA.”

Conclusions: “In addition, we conclude that more studies are required to fully understand how HOM yield and composition in aromatic systems depends on OH concentration and how the differences in HOM will affect the rate and magnitude of SOA formation. It would be valuable to sample different time scales, low and high reactant concentrations as well as effect of other important parameters, such as the effect of lights and NOx”

The bottom lines appear to be, 1) HOMs from aromatics are confirmed and 2) when constructing an laboratory-based model, everything matters. If the authors could extend their message to how their findings relate to HOM formation from biogenics (both in terms of magnitude and sensitivity to chamber conditions), which is comparatively well-studied and which has been implemented in some large scale models, it might enhance the narrative.

R2. We agreed with the reviewer and added a paragraph about the comparison to biogenic HOM studies in the end of section 4.2.1.:

"In comparison to biogenic VOC, our results were closest to the HOM yields observed in ozonolysis of α-pinene and limonene, 3.4-7% and 17% respectively (Bianchi et al. 2019). In the biogenic systems, especially if a VOC contains an endocyclic double bond, the first oxidation step by O_3 is known to form HOM at large yields. On the other hand, the observed yields in first-step OH oxidation are reported to be low (~1%, Bianchi et al. 2019). To our knowledge, no studies exist that explore HOM yields of biogenic VOC oxidation as a function of OH concentration. However, McFiggans et al. (2019) indicated a non-linear increase of HOM concentration with increasing α-pinene oxidation rate. We would therefore expect that also in biogenic systems, an increase in HOM yield due to multi-generation OH oxidation could be observed."

A key point I was missing was the authors' interpretation of how important these processes are in and downwind of the urban atmosphere. Do they have some idea if aromatic oxidation can be a substantial source of ultrafine particle formation events, or is it still too early to tell?

R3. Based on our laboratory results alone, it is not possible to tell what will be the contribution of these HOM to ambient particle formation, i.e. cluster formation. However, based on previous studies of HOM as well as our SOA experiment results, it is reasonable to think that these HOM are low-volatility compounds, which in the ambient atmosphere will be able to condense onto small aerosol particles. Clearly, as we also see HOM production in presence of NOx and we know other aromatics also produce HOM (Molteni et al. 2018, Wang et al. 2017, Hammes et al. in review), these compounds will be important players in particle growth and SOA formation where aromatic VOCs are abundant.

We added to *Summary and Conclusions*:

"Based on current understanding of HOM as well as our SOA experiment result, we can suggest that HOM observed in this study may play an important role in initial particle growth in ambient atmosphere where aromatic VOCs are abundant."

Specific Comments

1. Definition of molar yield: I appreciate the authors decision to use an operational definition of HOM yield, which is more in line with traditional methodologies for estimating SOA formation in large-scale models. In the short term, this option is easier to transcribe into models. However, the cost is that it is harder to account for sensitivity to environmental conditions like OH and NOx and translate chamber residence time to variable model time steps. Clearly, this approach of lumping the multigenerational formation together with the prompt formation is more suitable for aromatic VOCs (a point the authors make), but the timescale for this formation given on Page 19, line 9-10 is 10 h – 15 days. Some global models run with chemistry time steps on the order of tens of minutes to multiple hours. But regional models can be in the range of 5 minutes down to 45 seconds for high resolution cases. And LES models are even faster. Can the authors please consider discussing this aspect of how their data will be used? Are yields defined in this way really useful to large-scale models or are they more useful to other experimental efforts trying to constrain the total HOM formed.

R4. We would like to mention that our data set is too limited and the reviewer's requests for generalizations are beyond the scope of this experimental study. The absolute HOM yield values are mainly useful for other experimentalists to plan and interpret their studies, while the overall message that HOM yield and composition depends on OH is useful for experimentalists and modelers alike. Please see also the response R1.

2. The authors' point that OH and NOx should be considered when predicting HOMs from aromatics is well-taken; they have demonstrated it well. However, can they provide a parameterization for these effects that can be explored by other groups. The only option they have left the reader with is to interpolate the data in Table 1. If the authors do not think such a parametrization would be helpful, please discuss why.

R5. Please see responses R1 and R4 above. We have performed only one experiment with NO_X, which was good to demonstrate that NO_X should be considered, but not sufficient to formulate parametrizations. A recent paper by Hammes et al. (in review), discusses NO_X dependence of HOM formation in TMB in more detail. For yield dependence on OH/VOC/JO1D, all data is provided in Table 1, which can be used by other groups for comparison. These results are valid for a certain range of studied concentrations and the system appears that simple parametrizations are not so easy: the reaction system is too complex.

In addition, we added a short clarification to the discussion in section 4.2.1.:

"It should be noted that the specific dependency of HOM yield on OH may vary if other gases and loss mechanisms would be present."

3. Section 3.5: I recommend adding a table of all of the HOM molecules considered for the kinetic model of the seed experiment, to the appendix or supplemental. Are ions reported because multiple formulae apply to one ion in some cases? Equations 6, 7, and 8 indicate the kinetic model needs molecular weight and diffusion coefficent in air of every species of interest. If so, these parameters could be reported as well. I also recommend adding the formula to each of the sub-panels in Figures A1 and A2.

R6. The peaks used for the kinetic model in seed experiment (Figures A1 and A2) are identical to the ions used for HOM yield calculations. The list of them is presented in Table S4 in Supplement under "Non-nitrogen containing HOM". We identified the composition of ions using high resolution peak fitting and chose the peaks that were mainly single peaks for calculations, meaning other ions had minor contribution to the peak at this mass (see section 3.2.1 of the main text). We then performed unit mass resolution analysis for calculating HOM concentration (meaning we integrated the signal over the chosen peaks), and therefore we chose to show values for m/z in Figures A1 and A2 instead of ion composition. The ion composition at a specific mass can be found from Table S4.

In Equations 7 and 8, M_i was determined as the mass of the observed peak minus the mass of NO_3^-, if the molecule was clustered with NO_3^-.

We have made few modifications to make these clearer:

1. In Methods:

"If a HOM molecule was detected as cluster with NO_3^-, M_i was calculated as the m/z value of the peak minus the mass of NO_3^-. For this model, we used the peaks corresponding to the same HOM molecules as in the

HOM yield calculation, 69 peaks in total. The list of the m/z values and corresponding compositions can be found in Table S4 in Supplement."

2. In caption of Figure A1/A2

"Figure A1. Evolution of measured and modelled HOM monomers during the seed addition experiment. The list of HOM compositions for each peak at corresponding m/z is presented in Table S4 in Supplement."

"Figure A2. Evolution of measured and modelled HOM dimers during the seed addition experiment. The list of HOM compositions for each peak at corresponding m/z is presented in Table S4 in Supplement."

3. In caption of Table S4 in Supplement.

"Table S4. Peaks identified in JPAC. Non-nitrogen containing HOM were included in HOM yield calculation and kinetic model for seeded experiment…"

Indeed, in Equation 6, a diffusion coefficient is needed. Diffusion coefficient was approximated as 0.06 cm^2/s using an approximate value for weighted mean molecular weight 237 g/mol and diffusion volume as 170 based on method described by Fuller et al. 1966.

We corrected the text in methods to clarify this:

"D was approximated as 0.06 cm^2/s based on the mean molar mass 237 g/mol and approximated diffusion volume 170 of the observed HOM, according to the approach described by Fuller et al. 1966."

4. Page 15, line 9: HOM molar yield is set to 5%? Apparently I am confused about this model. I was under the impression that each HOM molecule would have a specific yield based on its relative abundance in the spectra from the base experiment. Is this not the case? Please consider explaining this portion of the approach clearer in the text.

R7. The reviewer's impression was correct, and we have modified the sentence in Methods to clarify that the "HOM molar yield" referred to the sum of all detected HOM molecules in the spectra:

"The molar yield of total HOM was set to 5% to match the measured HOM concentration before seed addition. For an individual HOM_i, the relative abundance in the spectra determined its yield."

5. The authors connect their experiments to previous SOA studies to try to explain the variability seen in the literature with what they have learned about HOMs. But the only parameter discussed is seed aerosol concentration. Are there any other features of HOM formation the authors think are connected to the apparent variability in historical SOA yields?

R8. We observe increase in HOM molar yield with an increasing OH. At the same time, we see that HOM readily condenses onto the seed aerosol and contributes to SOA formation. This means that variability in HOM will affect the formation of SOA. With our results, we could for example explain why at lower VOC concentrations in toluene oxidation Chen et al. (2019) observed larger SOA yields. At lower VOC concentration, there was more OH available per molecule of VOC likely allowing for HOM formation due to multi-generation OH oxidation. They performed SOA experiments without seed addition, so low-volatility compounds were needed to drive the growth of small particles.

Drawing more general conclusions is hard as many SOA studies do not investigate OH effect in detail. In addition, some studies lack wall loss corrections. Therefore, we cannot readily decouple many parameters affecting SOA yields reported in the literature. In context of SOA studies, we expect that HOM influence will be most visible for unseeded SOA formation as well as when seed is injected at low concentrations (Ehn et al. 2014). Therefore, in those experiments, we would expect SOA to depend on OH as well.

We added to the end of section 4.2.4 an explanation how we think our result in HOM will affect SOA:

"Based on our current understanding of HOM and the results from our SOA experiment, we expect that the change of HOM yield with OH would affect in turn the formed SOA yield. It is likely, that this effect will be mainly pronounced in SOA studies conducted without seed aerosol or in studies where seed aerosol is added at low concentrations (Ehn et al. 2014)."

Typos/Suggestions

1. Table 1 caption: quadrupole?

R9. We fixed this.

2. Page 13, Line 6-7: Are you reporting SOA yields in this work?

R10. We report SOA yield of 40% during the seeded experiment in section 4.2.4.

3. Page 14, Line 5-6: Please provide an equation relating k_loss to k_wall and CS.

R11. We added the equation to the text: k_loss = k_wall + CS.

4. Page 14, Line 27-29: What is the magnitude of uncertainty introduced from unidentified or omitted peaks?

R12. In Figure 5a and b, peaks included into yield calculation constitute ~50% of the signal between masses 200 and 550. This means that the yield can be potentially underestimated by a half. We included this into the text:

"As stated earlier, only clearly identifiable peaks were utilized for HOM concentration calculations, in order to make the quantification as robust as possible. These peaks constituted approximately 50% of the total signal in mass range from m/z 200 to 550. Although isotopes account for some of this unexplained fraction, our approach may cause an underestimation of the HOM yields by up to 50%."

5. Page 22, Line 9-11: Please rewrite this sentence to make it clearer that "total mass loading" is total PM mass (organic + inorganic) and that the percentage numbers are relevant to the organic only mass. There's nothing incorrect about this as-is sentence, but it could be reordered to make it easier for the reader to digest quickly.

R13. We re-wrote the sentence as follows:

"In the Ehn et al. (2014) experiments, the total aerosol mass loading was 30 µg m^{-3}, out of which 7 µg m^{-3} was the SOA mass formed during the experiment. The condensed HOM explained more than 50% of that SOA mass. In our benzene case, at total aerosol mass loading of 22 µg m^{-3}, the removed HOM explained around 30% of the 2.7 µg m^{-3} SOA mass."

Page 23, line 2-3: This statement "This clearly suggests. . .compete with CS." has been shown in other studies documenting the effect of seed aerosol and they should be referenced.

R14. We have added references as follows:

"This clearly suggests that aerosol loadings can greatly influence SOA yield estimates from chamber studies as long as wall loss can compete with CS (Ehn et al. 2014, Kokkola et al. 2014, Zhang et al. 2014)."

6. Figures A1 and A2: Do the authors have an explanation for the range of variability observed for different m/z. Some of them are relatively smooth, and others change wildly. Are the latter intermediates?

R15. The effect is simply due to differences in the absolute abundance of the different m/z, with low-signal m/z appearing more noisy.

Response to Anonymous Referee #1

General comments
Overall, this paper has shown that OH + aromatics (mainly benzene) produce a significant amount of highly oxidized molecules (HOM) that act as a reservoir for particles. OH + VOC (aromatics) ⇒ HOM ⇒ particles HOM are an array of compounds (with 6 or more O) that are the result of initial OH addition to the aromatics. Good evidence is provided that given enough time multiple OH reactions can take place and produce a larger array and amount of HOM. The challenge for this type of work is how to parameterize the data. In the abstract, they ask the modellers to consider these reactions, but this will only happen if such results are parameterized. At the moment this type of study is only semi-quantitative, i.e. there is an explanation for the HOMs but no rate coefficients. THIS IS THE BIG CHALLENGE.

R16. Please refer to the response R1.

Until a quantitative model is developed there is a problem of knowing which study is closest to atmospheric conditions. The study by Molteni(2018) indicated that HOM yields for benzene are 0.1-1% but in the present study, the yields are much higher 4 – 14%. Which is the correct result for atmospheric modelling? Are both studies in agreement, but it is the conditions that produce different yields?

R17. Molteni et al. (2018) provided a value of 0.2% for HOM molar yield in oxidation of benzene. Their experiment is conducted at shorter residence time and corresponds to mainly first and some second OH oxidation steps, as is supported by their HOM composition. Our flow reactor experiments are closer to the set-up of Molteni et al. and so is the HOM product distribution. We could not quantify our flow reactor results, however. Our results for HOM yield in JPAC chamber, on the other hand, correspond to HOM formed over long residence time, allowing for sequential OH oxidation steps, and also for slower isomerization reactions propagating the oxidation sequence. Therefore, the results are not in contradiction, but are relevant for different regimes. To provide parametrisations for atmospheric models, more studies on both long and short time-scales at atmospherically relevant concentrations are needed.

We modified and re-arranged the text in section 4.2.1 where the yields are compared, also including the issue with different timescales:

"Our estimated HOM yields from benzene oxidation were 4.1-14.0%, which can be compared to a value of 0.2% provided by Molteni et al. (2018). The difference in the results is expected due to the substantial

difference in the studied timescales (20 second in their study). In addition, in their flow reactor, air parcel was exposed to an initial OH concentration that decreased as OH reacted away, while in JPAC, the OH was produced continuously. This resulted in different OH doses in the systems. Considering these differences, less oxidation steps would be expected in a flow reactor. As a result, the yield in Molteni et al. (2019) likely corresponds to the HOM yield of the first OH oxidation step, potentially also impacted by a second step. This suggests that more than 90% of the "HOM- forming potential" of benzene comes from multi-generation OH oxidation in combination with slower isomerization reactions that may not be observed on shorter time scales."

We also added short clarifications into *Methods* and *Results and Discussion* about an OH dose:

"The OH concentration integrated over the residence time defines an OH dose, which could be used to compare the results with other systems or atmosphere. By definition, the OH dose would recognise that a 48-minute experiment with OH concentration of 10^8 cm^{-3} is equivalent to a 480-minute experiment with OH concentration of 10^7 cm^{-3}. Since in our JPAC experiments the residence time is kept constant, we use the OH concentration to describe our system."

Specific comments

page 7, 8 "Hydroxyl radicals were produced via photolysis of water at 184.9nm." I would make it clear that for each OH produce there is an HO2 (H + O2). This means in this reactor RO2 + HO2 is going to be significant and potentially suppress HOM formation. In the JPAC, OH is from O3/H2O (254nm) so only makes only OH

R18. We agree that in our flow reactor HO_2 formation is considerable. With each OH, we co-produce HO_2. On the other hand, each OH will also produce RO_2 through VOC oxidation. We can see that RO_2+RO_2 reactions are also important in our reactor as we can see HOM dimers. In the flow reactor, we still see HOM with 13 oxygen atoms, suggesting that autoxidation was fast enough to compete with bimolecular termination reactions.

We modified the text in the section 4.1 to reflect this:

"In photo-oxidation of any VOC, HO_2 production from RO_2 is efficient. HO_2 will also be co-produced from water photolysis in our reactor making a reaction with HO_2 an important bimolecular termination pathway. This is supported by the observation of $C_6H_8O_7$, $C_6H_8O_9$, $C_6H_8O_{11}$ and $C_6H_8O_{13}$. However, high oxygen content of HOM as well as the existence of dimeric species shows that the termination of RO2 by HO2 was not a dominant process in our system."

page 7, 10 "uncertainties in the VOC and OH concentrations were large enough that no quantitative analysis was attempted" Below an estimate [VOC] is made, so can an estimate of OH be made? What is [H2O] approximately?

R19. Unfortunately, we cannot estimate the OH concentration as the intensity of the lamp is unknown and thus the water photolysis rate cannot be determined.

page 8, 12 "The UV lamp (Philips, TUV 40W, λmax = 254nm) was located inside the chamber and was shielded from both ends with UV-absorbing glass tubes." How even is this light distributed in the chamber?

R20. The light distribution in the JPAC chamber is not completely even. Direct measurement of OH by LIF showed that the OH concentrations at the further end of JPAC were ½ of the average OH concentration determined by VOC consumption measurements (method applied here). However, the chamber is constantly stirred (mixing time < 2min) which ensures that the reactants see on average the same OH field.

From Figure 2, it takes 5 hours before reaching steady-state. Is this time to SS representative of all the experiments? If I understand correctly, you are waiting for

OH + VOC (aromatics) ⇒ HOM ⇒ particles

to reach steady-state and the MS data is only analyzed once SS is reached? Is there valuable data in the first 5 hours? If the HOM ratios are changing during this build-up time there should be further clues to the HOM formation mechanism? In the Helsinki experiments you have not reached SS, so where along this HOM concentration curve is applicable? DOES ANYONE HAVE A KINETIC MODEL TO EXPLAIN FIGURE 2?

R21. It is true that we limit our analysis to steady-state conditions. This is mainly because when lights are turned on we have a fast new particle formation and fast changes in ozone, OH, HOM and particle concentrations. In addition, modelling of gas-particle partitioning would require the knowledge of lower oxygenated compounds, information we do not have. Therefore, we would not be able to disentangle these different effects on HOM formation before steady state is reached. The time to reach SS in JPAC depended on how many particles were formed, and in high VOC experiments, it typically took ~5h. We cannot directly put the result of the flow reactor to the chamber HOM curve (if reviewer means Figure 2) as the both the reaction system and time scales are different (initial OH in flow reactor that reacts away versus OH produced constantly in JPAC) different.

In Equation 5, γ is in the denominator.
R22. We fixed the equation.

page 15, 4 “for each HOM molecule i" Can you indicate the value of i, i.e. how many HOMs are considered?
R23. Please see response R6.

page 16, 8 “HO2 can also be produced in our reactor making a reaction with HO2 an important bimolecular termination pathway in our system.” Please make in clear in the experimental that HO2 is made from H2O photolysis.
R24. We added this to the Methods:
“Hydroxyl radicals were produced via photolysis of water at 184.9nm, a reaction that also caused the co-production of HO_2”

Is there any specific reason that 185 nm was used to generate OH. If 254 nm and O3/H2O was used then there would be a more direct comparison to the JPAC experiment. Can the lamp be translated along the reactor to change the contact time? I note that Molteni(2018) used an excimer lamp at 172 nm. Both 185nm and 172nm will photolyze aromatics, but this is not the case for 254 nm.

R25. We performed the flow reactor experiments before JPAC, and with our existing hardware, we were limited to the 184.9nm light source.

The results in Figure 3 show that a range of HOMs are formed and the text provides some explanation of the type of reactions required to make each HOM. I was wondering if this could be quantified further. For instance, the dimers require an RO2 + RO2 bimolecular reaction. What sort of rate coefficient is required? While you state you do not know OH concentrations in the Helsinki experiments this makes it a difficult question, but in the JPAC experiments maybe this is possible.

R26. In JPAC experiments, the estimation of rate coefficients would be impossible primarily for two reasons: firstly, the long residence time and the fact that we cannot distinguish between RO_2 produced in different generations of OH oxidation; and secondly, a given ROOR likely has many isomers, and each RO_2 + RO_2 pair will have different reaction rates (as shown e.g. by Berndt et al. 2018).

page 18, 13 "The OH production from H2O photolysis stayed constant in our experiments, but the VOC acts as a sink for the OH radicals, which means that higher VOC concentrations will result in lower OH concentrations." Is there a reason why benzene or toluene was not lowered to maybe promote 2 OH reactions? If you had the bubbler before the MFC would you have greater control of the [VOC]?

R27. The main reason is because flow reactor experiments were conducted before JPAC, where we realized the effect of multi-generation oxidation on the formation of HOM. In addition, we operated at the smallest possible flows of MFC, 1 mlpm, meaning smallest VOC concentrations possible. On the other hand, it would be very difficult to generate higher OH in such a short time scale system without triggering other reactions that would obscure the multigeneration oxidation (for example, RO_2+OH recently receiving considerable attention).

Since, MFC requires a few bars pressure, placing a glass bubbler before the MFC would pressurize the bubbler.

In the Helsinki experiments, if the residence time could be changed then the mechanism of how these HOMs are formed might be clearer and even provide some kinetic assignments. If the lamp was located further along the reactor would this significantly change the residence time?

R28. As mentioned before, at the time of flow reactor studies we did not realise all the relevant aspects of HOM formation in aromatic system. The effect of residence time would be very useful in order to elucidate more exact mechanistic details of the oxidation reactions, but is outside the scope of this work, where we focus on the effect of multi-step OH oxidation on HOM formation.

Page 18, 31 "At small oxidation rates, the total HOM concentration increased linearly, but reached a plateau around 3-4 × 10^8 cm^{-3} at higher oxidation rate." This plateau is true for the light green square but not for the dark blue!

R29. As discussed later in the same section, plateau is reached for certain high VOC experiments (lower OH, lighter green in Figure 4a). This is due to the high amount of particles formed in those experiments.

We rephrased the sentence:

"In benzene experiments at small oxidation rates, the total HOM concentration increased linearly, but a plateau around 3 × 10^8 cm^{-3} was visible at higher oxidation rate."
"However, especially in the high [VOC] experiments (markers on the right hand side of Fig. 4a), the CS

due to particles formed in the chamber was of the same order as the wall loss and thus the approximation that k_{loss} equals k_{wall} is not valid anymore."

From Figure 4 b, HOM yield appears to be linear in OH. Surely there must be a limit where the HOM yield plateaus? If the HOM yield is increasing with more multiple OH reactions, does this mean that HOMmulti ⇒ particles is slower?

R30. We would like to point out that x-axis in Figure 4b is in logarithmic scale and, therefore, the yield dependence on OH is not linear. It is definitely the case that HOM yield will reach a plateau at some OH concentration. We, however, did not reach such a condition in our experiments.

"HOMmulti ⇒ particles is slower" – we assume the reviewer means that the formation rate of SOA would be slower because multiple oxidation steps must take place before the products become condensable. This delay in SOA formation has been observed in high NOx benzene oxidation experiments by Ng et al. (2007), but no delay was seen in no-NOx SOA experiments. In our SOA experiments, we would not be able to observe a delay because we introduced seed aerosols when the system was in steady state, while Ng et al. (2007) switched the oxidation on when seed concentration reached steady state. The HOM condensation and SOA formation at atmospherically-close concentration is highly non-linear especially as seed aerosol is in competition with wall loss. In addition, the rate of SOA formation will depend largely on how much of seed aerosol is added and what is the total concentration of condensable vapours and may not directly depend on the yield of HOM unless it is a nucleation SOA experiment (in absence of seed).

Page 19, 11 "Our estimated HOM yields from benzene oxidation were 4.1-14.0%, which can be compared to a value of 0.2% provided by Molteni et al. (2018). Their value likely corresponds to the HOM yield of the first OH oxidation step, potentially also impacted by a second step, suggesting that more than 90% of the "HOM- forming potential" of benzene comes from multi-generation OH oxidation." I'm confused here as to which study is relevant to the atmosphere. Molteni(2018) had a factor of ten less HOM than the present study, is this consistent with the OH concentration they used in their experiment? Which HOM yield would go into a model? Can you provide more discussion in the paper about this difference? Have you artificially raised the [OH] in order to bring about large [HOM]?

R31. Please refer to response R1 and R17.

The key differences between flow reactor (as in Molteni et al.) and continuous flow chamber studies (as in JPAC) is that in the former, the air parcel is provided with an initial OH concentration, which then reacts away as the parcel moves down the reactor. In the continuous flow chamber, however, we constantly produce OH during the 48 min residence time of the air inside. Therefore, OH concentrations cannot be directly compared. Instead, OH dose would be more appropriate value as it also takes into account the residence time. The initial concentration of OH in Molteni et al. was 8.5×10^{11} cm^{-3} and VOC concentration was about 4ppm, while in our study OH was 10^{7}-5×10^{8} cm^{-3} and VOC concentration was 1-100 ppb. Technically, the concentrations in our experiments were closer to the atmospheric values, but in terms of studying HOM yields, both studies are relevant, as the result is a function of reaction timescales.

"Have you artificially raised the [OH] in order to bring about large [HOM]?" – We conducted the experiments, in which we did produce OH artificially, with the aim of seeing the response at higher OH dose.

If you looked at the HOMi signal at early times, the 5 hours before steady-state, can you see the various HOMi evolving in time?

R32. Please refer to response R21.

Now if you are saying that the HOM yield is 10 times smaller for 1 OH reaction, then should the HOM spectra dramatically change, i.e. big difference between Figure 3 and 5?

R33. We discuss this difference in HOM composition in section 4.4.2. There are clear differences between Figure 3a and Figure 5a-c. The change is not very dramatic since the composition of secondary products, such as phenol and chatechol, have similar C and H content as benzene; however, the change is significant.

Page 21, 1 "However, after this, OH oxidation can only proceed via H-abstraction, and if the subsequent termination reactions occur by loss of OH or HO2, a decrease in H-atoms will take place. In other words, it is to be expected, that multi-generation OH oxidation will produce also molecules with fewer H-atoms than the parent VOC." Are these high [OH] HOM relevant to the atmosphere?

R34. If these intermediates, precursors for HOM, are semi-volatile, they may remain in the gas-phase in the atmosphere long enough to react several times with OH, which is equivalent to our high [OH]. A given VOC molecule receives in our experiments the same OH dose as a VOC molecule in the atmosphere over a course of 10 hours to 15 days. Therefore, the observed HOM are expected to be relevant to the atmosphere. Please also see response R17 in relation to OH dose.

Page 21, 3 "Another possibility is that the dimer formation upon RO2+R'O2 reaction would be less likely for the RO2 formed at high OH." I would have thought RO2 + RO2 is more likely the higher the OH concentration.

R35. Here we discuss the ratio between dimers and monomers. The formation of dimers will depend on RO2 concentration as well as on the dimer formation rate constant. If at high OH concentration, the RO2 structure is such that the dimer formation rate constant for is lower, then it could explain the observed decrease in dimer-to-monomer ratio. We clarified the sentence:

"This may be explained by higher HO2 concentrations at higher OH. Another possible explanation is that RO2 formed at higher OH would have less favourable structures for dimer formation. The dimer formation rate has been shown to be highly dependent on the structure of the reacting RO2 (Berndt et al., 2018a)".

Page 23, 22 "but also for some precursors for multi-generation HOM formation that are undetected by our instrument (or detected at lower sensitivity)." But I thought you are saying that the multi-generation HOM are from the primary generation HOM.
OH + HOMprimary ⇒ HOMmulti
What sort of intermediate before HOMmulti do you think might be present that is not detected? I understand why BPR is not detected but not what you are presently suggesting.

R36. We have realized that using the term "multi-generation HOM" could be misleading and changed it to "HOM formed in multi-generation OH oxidation". The specific sentence was changed as follows:

"but also for some of the undetected oxidation products (or detected at low sensitivity), that could have formed detectable HOM upon further OH oxidation steps. This explanation is plausible and is in support of our hypothesis that some of the HOM were formed in multi-generation OH oxidation."

If HOM formed in multiple OH oxidation steps was from other HOM that we could observe, we would not observed an increase in HOM yield. The increase in HOM molar yield tells us that some HOM were formed from lower-oxygenated compounds that we cannot detect (e.g. phenol, catechol, etc) or from those that we detect with lower sensitivity, or both. Currently, it is impossible to tell the following oxidation steps of which compounds form HOM. From Hyttinen et al. (2015), we know that even if a compound has 6 oxygen atoms and two H-donor functional groups, it does not mean it will necessarily be charged at collision limit in our chemical ionization inlet.

In section 4.2.1 we have included a short clarification what we mean under HOM formed in multi-generation OH oxidation:

"Since the observed HOM molar yield increased, we can conclude that the undetected lower oxygenated products reacted again with OH to form more of the detectable HOM. These intermediate precursors could also be higher oxygenated compounds that were detected in our instrument with ionisation efficiency below the collision limit (Hyttinen et al. 2015).
…
To test secondary OH oxidation, we conducted three similar experiments starting with phenol as the precursor, a known first-generation oxidation product of benzene."

Page 24, 30 "In addition, we conclude that atmospheric models should take into account HOM yield dependence on the chemical regime when implementing quantitative laboratory results." Can you make it clear which study is relevant to the atmosphere, the present work (high HOM yield) or Molteni(2018) (low HOM yield).

R37. Please refer to response R1.

References:

Berndt, T., Mentler, B., Scholz, W., Fischer, L., Herrmann, H., Kulmala, M., and Hansel, A.: Accretion Product Formation from Ozonolysis and OH Radical Reaction of α-Pinene: Mechanistic Insight and the Influence of Isoprene and Ethylene, Environmental Science & Technology, 52, 11 069–11 077, https://doi.org/10.1021/acs.est.8b02210, 2018.

Chen, T., Liu, Y., Chu, B., Liu, C., Liu, J., Ge, Y., Ma, Q., & Ma, J., and He, H.: Differences of the oxidation process and secondary organic aerosol formation at low and high precursor concentrations. Journal of Environmental Sciences. 79. 10.1016/j.jes.2018.11.011, 2018.

Hammes, J., Tsiligiannis, E., Mentel, T. F., and Hallquist, M.: Effect of NOx on 1,3,5-trimethylbenzene (TMB) oxidation product distribution and particle formation, Atmos. Chem. Phys. Discuss., 2019, 1-18, 10.5194/acp-2019-395, 2019.

Hyttinen, N., Kupiainen-Määttä, O., Rissanen, M. P., Muuronen, M., Ehn, M., and Kurtén, T.: Modeling the Charging of Highly Oxidized Cyclohexene Ozonolysis Products Using Nitrate-Based Chemical Ionization, The Journal of Physical Chemistry A, 119, 6339–6345, https://doi.org/10.1021/acs.jpca.5b01818, 2015.

McFiggans, G., Mentel, T. F., Wildt, J., Pullinen, I., Kang, S., Kleist, E., Schmitt, S., Springer, M., Tillmann, R., Wu, C., Zhao, D., Hallquist, M., Faxon, C., Le Breton, M., Hallquist, Å. M., Simpson, D., Bergström, R., Jenkin, M. E., Ehn, M., Thornton, J. A., Alfarra, M. R., Bannan, T. J., Percival, C. J., Priestley, M., Topping, D., and Kiendler-Scharr, A.: Secondary organic aerosol reduced by mixture of atmospheric vapours, Nature, 565, 587-593, 10.1038/s41586-018-0871-y, 2019.

Molteni, U., Bianchi, F., Klein, F., Haddad, I. E., Frege, C., Rossi, M. J., Dommen, J., and Baltensperger, U.: Formation of highly oxygenated organic molecules from aromatic compounds, Atmospheric Chemistry and Physics, 18, 1909–1921, https://doi.org/10.5194/acp-18-1909-2018, 2018.

Ng, N. L., Kroll, J. H., Chan, A.W. H., Chhabra, P. S., Flagan, R. C., and Seinfeld, J. H.: Secondary organic aerosol formation fromm-xylene, toluene, and benzene, Atmospheric Chemistry and Physics, 7, 3909–3922, https://doi.org/10.5194/acp-7-3909-2007, 2007.

Wang, S., Wu, R., Berndt, T., Ehn, M., and Wang, L.: Formation of Highly Oxidized Radicals and Multifunctional Products from the Atmospheric Oxidation of Alkylbenzenes, Environmental Science&Technology, 51, 8442–8449, https://doi.org/10.1021/acs.est.7b02374, 2017.

Multi-generation OH oxidation as a source for highly oxygenated organic molecules from aromatics

Olga Garmash[1], Matti P. Rissanen[1,2], Iida Pullinen[3,9], Sebastian Schmitt[3,10], Oskari Kausiala[1,11], Ralf Tillmann[3], Defeng Zhao[3,12], Carl Percival[4], Thomas J. Bannan[4], Michael Priestley[4,5], Åsa M. Hallquist[6], Einhard Kleist[7], Astrid Kiendler-Scharr[3], Mattias Hallquist[5], Torsten Berndt[8], Gordon McFiggans[4], Jürgen Wildt[3,7], Thomas Mentel[3], and Mikael Ehn[1]

[1]Institute for Atmospheric and Earth System Research / Physics, Faculty of Science, University of Helsinki, Helsinki, Finland
[2]Aerosol Physics Laboratory, Physics Unit, Faculty of Engineering and Natural Sciences, Tampere University, Tampere, Finland
[3]Institut für Energie- und Klimaforschung, IEK-8: Troposphäre, Forschungszentrum Jülich GmbH, Jülich, Germany
[4]School of Earth and Environmental Sciences, University of Manchester, Manchester, UK
[5]Atmospheric Science, Department of Chemistry and Molecular Biology, University of Gothenburg, Gothenburg, Sweden
[6]IVL Swedish Environmental Research Institute, Gothenburg, Sweden
[7]Institut für Bio- und Geowissenschaften, IBG-2: Pflanzenwissenschaften, Forschungszentrum Jülich GmbH, Jülich, Germany
[8]Leibniz-Institut für Troposphärenforschung (TROPOS), Permoserstraße 15, 04318 Leipzig, Germany
[9]Present address: Department of Applied Physics, University of Eastern Finland, Kuopio, Finland
[10]Present address: TSI GmbH, Aachen, Germany
[11]Present address: Kärsa Oy, Helsinki, Finland
[12]Present address: Department of Atmospheric and Oceanic Sciences & Institute of Atmospheric Sciences, Fudan University, Shanghai, China

Correspondence: Olga Garmash (olga.garmash@helsinki.fi) and Mikael Ehn (mikael.ehn@helsinki.fi)

Abstract.

Recent studies have recognized highly oxygenated organic molecules (HOM) in the atmosphere as important in the formation of secondary organic aerosol (SOA). A large number of studies have focused on HOM formation from oxidation of biogenically emitted monoterpenes. However, HOM formation from anthropogenic vapours has so far received much less attention. Previous studies have identified the importance of aromatic volatile organic compounds (VOC) for SOA formation. In this study, we investigated several aromatic compounds, benzene (C_6H_6), toluene (C_7H_8), and naphthalene ($C_{10}H_8$), for their potential to form HOM upon reaction with hydroxyl radicals (OH). We performed flow tube experiments with all three VOC, and focused in detail on benzene HOM formation in the Jülich Plant Atmosphere Chamber (JPAC). In JPAC, we also investigated the response of HOM to NO_X and seed aerosol. Using a nitrate-based chemical ionization mass spectrometer (CI-APi-TOF), we observed the formation of HOM in the flow reactor oxidation of benzene from the first OH attack. However, in the oxidation of toluene and naphthalene, which were injected at lower concentrations, multi-generation OH oxidation seemed to impact the HOM composition. We tested this in more detail for the benzene system in the JPAC, which allowed for studying longer residence times. The results showed that the apparent molar benzene HOM yield under our experimental conditions varied from 4.1 to 14.0%, with a strong dependence on the OH concentration, indicating that the majority of observed HOM formed through multiple OH-oxidation steps. The composition of the identified HOM in the mass spectrum also supported this hypothesis. By

injecting only phenol into the chamber, we found that phenol oxidation cannot be solely responsible for the observed HOM in benzene experiments. When NO_X was added to the chamber, HOM composition changed and many oxygenated nitrogen-containing products were observed in CI-APi-TOF. Upon seed aerosol injection, the HOM loss rate was higher than predicted by irreversible condensation, suggesting that some undetected oxygenated intermediates also condensed onto seed aerosol, which is in line with the hypothesis of ~~multi-generation HOM~~ that some of the HOM were formed in multi-generation OH oxidation. Based on our results, we conclude that HOM yield and composition in aromatic systems strongly depend on OH and VOC concentration ~~, we conclude that atmospheric models should account for such dependency and the chemical regime when implementing the quantitative results of laboratory studies~~ and more studies are needed to fully understand this effect in formation of HOM and, consequently, SOA. We also suggest that the dependence of HOM yield on chamber conditions may explain part of the variability in SOA yields reported in the literature and strongly advise monitoring HOM in future SOA studies.

1 Introduction

Highly oxygenated organic molecules (HOM) have been identified as large contributors to atmospheric secondary organic aerosol (SOA) in forested environments (Ehn et al., 2014; Öström et al., 2017; Bianchi et al., 2019). HOM form through a process called autoxidation, where intramolecular hydrogen shifts in organic peroxy radicals are followed by addition of molecular oxygen (Crounse et al., 2013), causing a rapid increase in the oxygen content of the molecules. The product is a new peroxy radical, with an additional hydroperoxide functionality, that may be able to experience additional H-shifts. A wealth of studies have shown that this process is especially efficient in the oxidation of molecules with endocyclic double bonds (e.g., Rissanen et al., 2014; Jokinen et al., 2014; Mentel et al., 2015; Berndt et al., 2015; Rissanen et al., 2015; Berndt et al., 2016), a feature typical of biogenically emitted volatile organic compounds (VOC) such as monoterpenes.

While the formation pathways of HOM from biogenic VOC as well as their impact on atmospheric aerosol formation has been studied extensively over the past years, the potential of anthropogenic VOC to form HOM has received much less attention. Wang et al. (2017) showed both computationally and experimentally that the yield of HOM from the hydroxyl radical (OH) initiated oxidation of alkyl benzenes increased with the size of the alkyl group. A second study investigated HOM formation from OH oxidation of seven different aromatics, finding HOM yields mainly within 0.1-1% for single-ring aromatics, and a few percent for two polycyclic aromatics, naphthalene and biphenyl (Molteni et al., 2018). These yields are comparable in magnitude with those reported from ozone and OH oxidation of monoterpenes (e.g., Jokinen et al., 2015; Berndt et al., 2016). As aromatics are thought to be the most efficient precursors of SOA in urban areas (Kroll and Seinfeld, 2008), further studies of HOM formation, as well as their contribution to SOA, are necessary.

The most abundant aromatics in the atmosphere are benzene and alkylated benzenes, i.e. toluene, xylenes and trimethylbenzenes. Their primary sources are traffic, fuel handling and industrial processes. Aromatic compounds can constitute up to 20% of urban VOC (Calvert et al., 2002) and in extremely polluted environments, such as next to a road with heavy traffic, their total concentrations can reach up to tens of ppb (Liu et al., 2008). In addition, vegetation also emits a wide range of aromatic compounds, often in oxygenated form, and the total amount of the potential emissions may even match the anthropogenic sources (Misztal et al., 2015).

The major sink of aromatics in the atmosphere is the reaction with OH (Atkinson and Arey, 2003), which in most cases involves OH addition to the aromatic ring and the formation of a carbon-centred radical. In the case of benzene, more than half of these radicals will end up forming phenol (Volkamer et al., 2002; Berndt and Böge, 2006). The remainder of the products can undergo O_2-additions and isomerisation, forming bicyclic peroxy radicals (BPR) or result in epoxides (Bloss et al., 2005; Glowacki et al., 2009; Wang et al., 2013). As suggested by Molteni et al. (2018), the BPR may undergo further autoxidation to form HOM. However, the produced phenol will be abundant, which upon reaction with OH can also produce a BPR with low yield, about 10% (Master Chemical Mechanism, MCMv3.3.1, Bloss et al., 2005). The reaction rate coefficient of phenol with OH is about 20 times higher than that of benzene, meaning that we cannot ignore its role in the total HOM formation following further oxidation steps. For instance, Schwantes et al. (2017) showed that methylphenol (cresol) formed in toluene oxidation was a much more important SOA precursor than its branching ratio (20%) would suggest. In their study, only a minor fraction of the identified compounds would classify as HOM according to the definition suggested by Bianchi et al. (2019), that six or more O-atoms are required for a molecule to be classified as HOM. However, the authors demonstrated the importance of multiple OH oxidation steps for SOA formation.

Several studies over the last decades examined the SOA yields from oxidation of aromatics, with disparate results that remain largely unexplained. The suggested causes are the differences in the exact experimental conditions (Ng et al., 2007; Hildebrandt et al., 2009; Emanuelsson et al., 2013). These include differences in VOC loading, UV light intensity, and the concentration of NO_X ($NO+NO_2$). Being a by-product of combustion, NO_X is on a large scale co-emitted with aromatic VOC. NO_X, and especially NO, will decrease the lifetime of RO_2 radicals in the atmosphere, in direct competition with autoxidation (Praske et al., 2018; Rissanen, 2018). Additionally, highly oxygenated RO_2 radicals can combine efficiently to form ROOR' dimers (Berndt et al., 2018a, b). These dimers are often the least volatile oxidation products, with a particularly large influence on the formation of new particles (e.g., Tröstl et al., 2016; Lehtipalo et al., 2018), but under high-NO_X conditions their formation becomes supressed (e.g., Ehn et al., 2014; Rissanen, 2018) .

The measurement of HOM relies mainly on the use of the chemical ionisation atmospheric pressure interface time-of-flight mass spectrometer, CI-APi-TOF (Jokinen et al., 2012). In combination with wall-less CI inlet, nitrate ion ionisation is typically used due to its selectivity towards molecules with several H-bond donors, such as the multi-hydroperoxides typically formed in autoxidation (Hyttinen et al., 2015). Until now, the application of the CI-APi-TOF to measuring HOM from aromatics has been limited to a few studies (Wang et al., 2017; Molteni et al., 2018), and these have been performed in flow reactors with residence times of 20 seconds or less. To understand the importance of aromatic-derived HOM in the atmosphere, systematic studies, including experiments at varying conditions and longer timescales, are needed.

In this study, we investigated the OH-initiated oxidation of aromatics, with a strong focus on benzene. We conducted experiments in a flow reactor and a continuously stirred tank reactor (JPAC) in order to determine HOM composition and yield over a wide range of conditions. In the JPAC runs, we varied both VOC and OH concentrations, and tested the influence of NO_X on the HOM distribution. Benzene was also substituted by phenol in order to test different oxidation pathways. Finally, we explored the contribution of HOM to SOA formation by adding seed aerosol.

2 Aromatic Oxidation Chemistry

In this section, we outline the relevant oxidation steps of aromatic compounds with a focus on benzene. In oxidation reactions initiated by OH, the oxidation propagation and termination will determine the chemical composition of the product molecules. These reactions will change the amount of hydrogen (H), carbon (C), oxygen (O) and nitrogen (N) atoms in the detected oxidised species and are therefore central to our discussion. In this section, we do not attempt to review all of the existing studies. Instead, we present an overview of relevant products and radicals formed in benzene oxidation by OH. We also discuss the relevant chain propagating and terminating reactions of organic peroxy radicals (RO_2) as the main intermediates of gas-phase oxidation. Detailed mechanistic descriptions of benzene oxidation can be found in the literature (Calvert et al., 2002; Volkamer et al., 2002; Bloss et al., 2005; Glowacki et al., 2009; Wang et al., 2013; Vereecken, 2019, and references therein).

2.1 Oxidation by OH

Benzene (C_6H_6) oxidation by OH almost exclusively initiates via addition of OH to the aromatic ring (Glowacki and Pilling, 2010; Bloss et al., 2005), while abstraction of H-atoms from the ring is a minor pathway. The addition of OH creates a carbon-centred radical C_6H_7O•. According to previous studies, about 53 - 61% of these radicals will form phenol, where the aromatic ring is retained and C_6H_6O molecule has one OH group (one more O atom) (Volkamer et al., 2002; Berndt and Böge, 2006). The remaining fraction of C_6H_7O• will add molecular oxygen (O_2) forming a $C_6H_7O_3$• peroxy radical (Lay et al., 1996). This RO_2 can undergo endo-cyclization, where RO_2 attacks its own double bond to form an oxygen bridge resulting in an alkyl radical. This radical then reacts again with O_2 and forms a bicyclic peroxy radical (BPR) $C_6H_7O_5$• (Glowacki et al., 2009; Birdsall et al., 2010; Wang et al., 2013). In this pathway OH attachment and addition of two O_2 increases the molecular composition of parent benzene by five O atoms (and one H), and subsequent reactions generally lead to radical termination, and potential molecular fragmentation (Jenkin et al., 2003; Wang et al., 2013). Studies have also reported a minor channel in which the $C_6H_7O_3$• bicyclic alkyl radical isomerises and forms an epoxide functionality, though the importance of this pathway under atmospheric conditions is yet unclear (Bloss et al., 2005; Glowacki et al., 2009; Wang et al., 2013).

For substituted aromatics, the set of reactions is similar to that described above, though branching ratios are different (Birdsall and Elrod, 2011). For instance, in toluene oxidation by OH, the BPR forms with about 65% yield, which is about twice that formed in the case of benzene (MCMv3.3.1, Bloss et al., 2005). In addition, the presence of methyl groups increases the chances of H-abstraction by OH radicals as well as increases the OH-VOC reaction rate coefficient (k_{OH}) (Bloss et al., 2005; Atkinson, 1994a, b; Atkinson and Aschmann, 1989).

A distinct feature of aromatic oxidation is the faster oxidation rates of first-generation products as compared to the parent molecule. For instance, benzene has a k_{OH} of 1.22×10^{-12} cm^3 s^{-1} at 298 K, while k_{OH} of phenol is about 20 times larger, 2.82×10^{-12} cm^3 s^{-1} 10^{-11} cm^3 s^{-1}, and k_{OH} of catechol (a primary product of phenol oxidation) is about 100 times higher (1.0×10^{-10} cm^3 s^{-1}) (Atkinson et al., 2006). In the case of less thoroughly investigated oxidation products, k_{OH} is likely to increase in comparison to benzene itself, as the pi-electron structure of benzene makes it less susceptible towards OH oxidation compared to most organic molecules. The process of sequential oxidation is commonly known as ageing and in general should lead to eventual fragmentation of the products retaining in the gas phase (Chacon-Madrid and Donahue, 2011).

2.2 RO_2 radical reactions

2.2.1 Chain propagation

Chain propagation refers to the reactions that result in another radical (i.e., still has an unpaired electron). These reactions can be bimolecular, happening upon collision with another molecule, or unimolecular, occurring within the molecule. The reaction rates depend on the structure of the compound as well as the concentration of potential bimolecular reaction partners.

A bimolecular propagation reaction proceeds through formation of alkoxy radicals (RO) when an RO_2 radical reacts with another $R'O_2$ (forming $RO+R'O+O_2$) or NO (forming $RO+NO_2$). This reaction decreases the oxygen content per molecule by one and is one of the most common reactions for peroxy radicals (Finlayson-Pitts and Pitts, 2000). The fate of the RO radicals depends on their structure. They can decompose, undergo H-shifts, or react with O_2. In case of benzene, decomposition of alkoxy radicals may lead to ring scission and potentially further autoxidation. However, in case of first-generation BPR from benzene, the Master Chemical Mechanism (MCMv3.3.1) predicts that BPR will react with HO_2 or RO_2 forming RO radicals with branching ratios of 23% and 60%, respectively, and eventually decompose into smaller molecules (Jenkin et al., 2003; Bloss et al., 2005).

Autoxidation of RO_2 radicals is one important reaction chain recently shown in oxidation of monoterpenes and other alkenes (Crounse et al., 2013; Ehn et al., 2014). It involves intramolecular hydrogen shifts to the peroxide group from other carbon atoms and subsequent addition of oxygen to the produced carbon-centred radicals. While autoxidation involves both uni- and bimolecular reactions, the high abundance of oxygen in the air allows autoxidation to be pseudo-unimolecular (Rissanen et al., 2015). Autoxidation is more likely to happen at lower RO_2 concentrations and for RO_2 with larger amount of functional groups (Crounse et al., 2013). It may also occur in aromatic molecules following the initial bicyclic peroxy radical, i.e. $C_6H_7O_5$• in case of benzene (Wang et al., 2017). H-shift itself does not modify the molecular composition, but O_2 additions increase the oxygen content by an even number. Autoxidation can proceed until the H-shift potential is exhausted and, at least in monoterpene systems, can often be competitive with bimolecular termination reactions at atmospheric conditions (see next section). However, autoxidation for aromatic compounds is not yet well understood, and until recently, the bicyclic peroxy radical was considered the most oxygenated first-generation product.

Other propagation reactions mostly include fragmentation. During autoxidation, H atoms may be abstracted from a terminal carbonyl group creating an acyl radicals (RC•=O), which may eliminate a CO from the molecule and leave an alkyl radical

where further O_2 can attach. In this reaction, one C atom and one O atom are lost (Crounse et al., 2012; Rissanen et al., 2014). If CO is not eliminated, O_2 will add and, upon a reaction with another RO_2 (or NO), an RO radical will split CO_2, losing one C and two O atoms instead (Orlando et al., 2003; Atkinson and Arey, 2003; Vereecken and Peeters, 2009).

2.2.2 Chain termination

Termination reactions proceed in competition with the chain propagation reactions described above. Termination reactions result in "closed-shell" molecules containing only paired electrons. An example of a unimolecular termination process is the ejection of OH following an H-abstraction from a carbon with a hydroperoxide group, forming a carbonyl (C=O), meaning a loss of one H and one O atom (Rissanen et al., 2014).

A number of bimolecular termination reactions can take place. First, RO_2 can react with HO_2, and form ROOH hydroperoxides, which adds one H atom (as O_2 is ejected). Alternatively, RO_2 can react with another $R'O_2$ and form a dimer ROOR' and O_2, where the number of C and H atoms of RO_2 and $R'O_2$ in sum are conserved, while two O-atoms are lost. RO_2 can also upon collision with $R'O_2$ form an alcohol (ROH) or an aldehyde (RCHO) and O_2 in which the molecule will have lost an oxygen and either gained or lost a hydrogen, compared to the initial RO_2 (Finlayson-Pitts and Pitts, 2000). In addition, RO radicals, mentioned in the previous section, may terminate upon reaction with O_2 forming a carbonyl compound with one less H atom.

In the atmosphere, NO and NO_2 can be effective in terminating RO_2, although the major reaction between RO_2 and NO is chain-propagating to form NO_2 and RO. NO can add to RO_2 to form organonitrates while NO_2 upon reaction with RO_2 can form thermally unstable peroxynitrates (RO_2NO_2) or more stable peroxyacylnitrates $RO_2(O)NO_2$ (Zabel, 1995; Atkinson, 2000; Orlando and Tyndall, 2012; Rissanen, 2018). In the case of aromatics, RO can also be long-lived enough to react with NO_2 to form nitrophenol-type compounds (Olariu et al., 2002; Jenkin et al., 2003; Bloss et al., 2005). NO and NO_2 addition to the molecule consequently changes its composition, and are easy to identify based on the added N-atom. However, separating between nitrogen-containing HOM with nitro-, nitrate- or peroxynitrate functionalities is impossible with our instrumentation, and can only be speculated based on experimental conditions like the NO/NO_2 ratio.

3 Methods

3.1 Experimental set-up

The gas-phase oxidation experiments were conducted in two different laboratory settings. Initial experiments were performed in a flow reactor at the University of Helsinki, focusing on determination of HOM distributions during the oxidation of benzene, toluene and naphthalene. The flow reactor allowed fast oxidation experiments at high VOC concentrations providing a possibility for comparison with previous studies. Motivated by the findings in the flow reactor, we performed subsequent quantitative studies on HOM formation from benzene oxidation at the Jülich Plant Atmosphere Chamber facility (JPAC) at Research Centre Jülich (Mentel et al., 2009). Using JPAC allowed us to do experiments at longer time scales and more var-

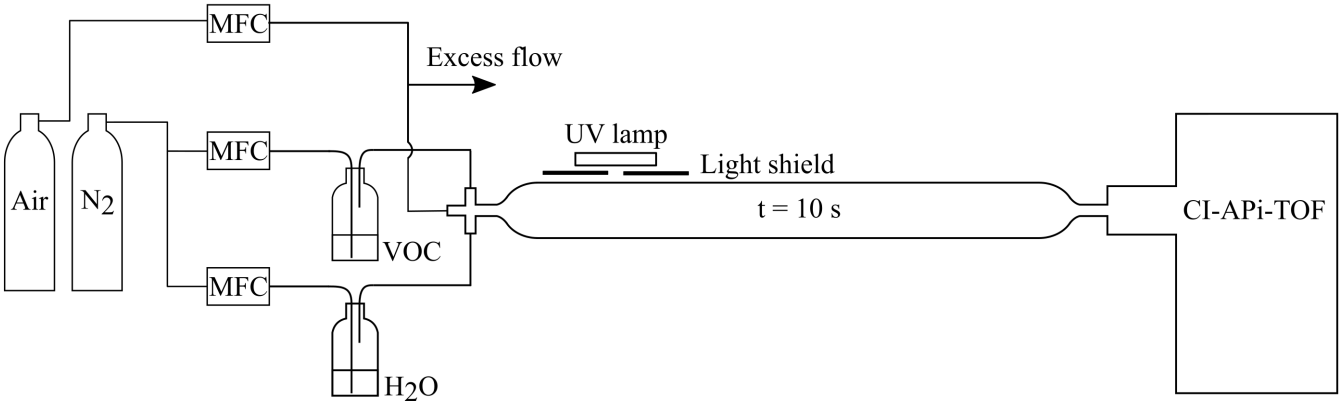

Figure 1. Flow reactor set-up used at the University of Helsinki. The aromatic VOC and water vapour were mixed with synthetic air at the inlet of the flow reactor. A shielded UV lamp irradiated a small part of the reactor, forming OH radicals by photolysing the water vapour. The inlet flow to the CI-APi-TOF mass spectrometer (see Sect. 3.2.1) defined the residence time (~10 seconds) in the reactor.

ied experimental conditions. In the following sub-sections, the two facilities are described in more detail, as are the types of experiments conducted in each of them.

3.1.1 University of Helsinki flow reactor

The flow reactor utilised in this work was made of quartz and had a volume of 2 litres. At the inlet of the flow reactor, reactant gases were mixed in a Swagelok steel cross. We operated the system at room temperature (~22 °C) with high VOC concentrations. Synthetic air (80% N_2/20% O_2; AGA purity 5.0, 99.999%) was used as the main carrier gas, while VOC and water were added via separate lines by bubbling nitrogen (cryogenic N_2, AGA) through vials containing the respective liquids (see Fig. 1 for a schematic depiction of the set-up). In the case of the solid naphthalene, nitrogen flow was passed over granules of the compound. An ultraviolet (UV) lamp was attached on the top of the reactor, irradiating a small part of it through a light shield. Hydroxyl radicals were produced via photolysis of water at 184.9nm, a reaction that also caused the co-production of HO_2. The total flow through the flow reactor was 12 standard litres per minute (slpm), leading to a 10 second residence time inside the reactor.

In the flow reactor experiments, uncertainties in the VOC and OH concentrations were large enough that no quantitative analysis was attempted, but instead we focused on the chemical composition of the HOM products. We could only roughly approximate the VOC concentrations in the flow reactor. Assuming the flow over the VOC in the vial (0.01-0.05 slpm) was saturated, we got the following estimated concentrations in the flow reactor for different experiments: benzene ~400 ppm, toluene ~25 ppm, and naphthalene ~0.4 ppm. The photolysis rate could not be determined in the present set-up, and thus no attempt was made to calculate OH concentrations in the flow reactor. We also conducted direct VOC photolysis experiment in absence of water to determine the effect of this process on the product spectrum.

3.1.2 Jülich Plant Atmosphere Chamber (JPAC)

In this study, we used the larger chamber of the JPAC facility (1450 l), made from Borosilicate glass (Mentel et al., 2009). It was operated as a continuously stirred tank reactor with modifications as described in Mentel et al. (2015). The chamber was positioned in a temperature-controlled housing and the temperature throughout the experiments was kept at 14.2 ± 0.3 °C. Purified air was fed into the system at a flow rate of ~30 l min^{-1} allowing a ~48 minute residence time. A slight overpressure of 5 mbar was maintained to reduce the leaking of ambient air into the chamber. Inflow to the chamber was from two separate lines, one used to feed ozone and humidified air, the other to introduce VOC and NO_X mixed into dry air. The RH in the chamber was maintained at 65 ± 3%.

Benzene was fed into the chamber from a diffusion source with a constant flow, and the concentration in the chamber could be varied according to what fraction of this flow was diverted into the chamber. The procedure was identical in the experiments where phenol was used instead of benzene. OH radicals were produced by ozone photolysis in presence of water vapour. The UV lamp (Philips, TUV 40W, λ_{max} = 254nm) was located inside the chamber and was shielded from both ends with UV-absorbing glass tubes. OH production could be varied by either adjusting the concentration of ozone or the light intensity by changing the size of the gap between the UV-absorbing tubes on the UV lamp. Starting ozone concentration was varied between 15 and 100 ppb resulting in OH concentrations 1.2 – 45 × 10^7 cm^{-3}. These parameters, together with the concentration of benzene, determined the final concentration of OH inside the chamber. The OH concentration integrated over the residence time would define an OH dose, which could be used to compare the results between different systems or atmosphere. By definition, the OH dose would recognise that a 48-minute experiment with OH concentration of 10^8 cm^{-3} is equivalent to a 480-minute experiment with OH concentration of 10^7 cm^{-3}. Since in our JPAC experiments the residence time is kept constant, we use the OH concentration to describe our system.

The influence of NO_X on the benzene oxidation system was studied by injecting NO into the chamber. The injected NO resulted in 4.3 ppb of NO_X. UV-A lights (12 x HQI, 400 W/D; Osram, Munich, Germany) around the chamber were used to photolyse NO_2 to NO and O, the latter reacting with O_2 to form ozone. Ozone consequently reacts with NO to reform NO_2. A photostationary state with a constant NO_2:NO ratio of roughly 3:1 was achieved at a given ozone concentration (~58 ppb) and photolysis rate (J_{NO_2}, ~4.2x10^{-3} s^{-1}).

In certain experiments, monodisperse 100 nm seed aerosol particles consisting of dry ammonium sulfate ($(NH_4)_2SO_4$, AS) were introduced into the chamber. The AS particles were formed by atomising an ammonium sulfate water solution, which were then dried using silica gel and size-selected using a differential mobility classifier (TSI Inc, 3071). Before particles were added, pure water was nebulised to ensure a constant flow into the chamber. The achieved aerosol had a bimodal distribution, as ~25% of the particles were doubly charged particles of larger size, which, having the same electrical mobility, entered the chamber. This was considered when calculating the condensational sink in the chamber (CS). The seed addition experiments helped assessing the amount of SOA that was formed from low-volatile compounds, as the increased CS shifted their main sink from the chamber walls to the aerosol. The method is described in more detail by Ehn et al. (2014).

Table 1. Summary of the experimental parameters from the JPAC chamber. QMS/TOF refers to ~~quadruple~~ quadrupole / time-of-flight detector in the proton transfer reaction (PTR) mass spectrometer used for measuring VOC.

benzene							
#	**PTR**	**UV lamp, J(O^1D), 10^{-3} s^{-1}**	**VOC, ppb**	**OH, 10^7 cm^{-3}**	**HOM, 10^7 cm-3**	**CS, s^{-1}**	**HOM yield, %**
1	QMS	2.6	4.5	25.4	30.6	$1.3x10^{-3}$	10.9
2	QMS	2.6	6.4	8.7	12.2	$6.8x10^{-6}$	8
3	QMS	2.6	6.5	8.5	12.1	$6.3x10^{-6}$	8
4	QMS	2.6	5.3	16.5	23.7	$4.5x10^{-4}$	10.2
5	QMS	2.6	4.1	29.5	34	$4.2x10^{-3}$	14
6	QMS	1.5	4.4	20.3	24.9	$2.7x10^{-4}$	10.4
7	QMS	2.6	3.7	29.1	30.8	$1.2x10^{-3}$	11.6
8	QMS	4.9	2.9	44.6	36.3	$3.3x10^{-3}$	13.2
9	QMS	3.8	3.1	42.6	36.2	$1.9x10^{-3}$	11.5
10	QMS	2.6	6.3	6.1	8.4	$8.0x10^{-6}$	8
11	QMS	2.6	2.5	6.1	4.6	$7.2x10^{-6}$	11
12	TOF	2.6	13.3	3.6	10.3	$1.3x10^{-5}$	7.9
13	TOF	2.6	30.4	2.6	13.7	$1.6x10^{-5}$	6.5
14	TOF	2.6	2.4	7.4	4.6	$9.8x10^{-6}$	9.4
15	TOF	2.6	1.6	10.6	4.1	$1.0x10^{-4}$	8.8
16	TOF	2.6	6.9	6	9.5	$9.0x10^{-6}$	8.4
17	QMS	2.6	112.4	1.2	19.5	$4.9x10^{-5}$	5.2
18	QMS	4.9	105.7	3.3	30.9	$6.8x10^{-3}$	5.3
19	TOF	4.9	95.1	4.7	30.6	$2.0x10^{-2}$	6.9
20	TOF	2.6	14.9	10.2	26	$4.1x10^{-3}$	8.5
21	TOF	2.6	14.5	10	26.3	$4.0x10^{-3}$	9
22	TOF	2.6	75.3	4	29.7	$3.8x10^{-3}$	4.8
23	TOF	2.6	94.9	2.9	30.8	$2.8x10^{-3}$	5
24	TOF	2.6	64.9	3.2	30.6	$2.3x10^{-3}$	6.4
25	TOF	2.6	84.1	2.6	32.1	$2.1x10^{-3}$	6.4
26	QMS	2.6	15.7	4.1	7.2	$9.4x10^{-5}$	4.1
27	TOF	1.7	16.1	5.9	22.2	$3.2x10^{-4}$	8.8

Table 1. Continued.

phenol								
#	**PTR**	**UV lamp, J(O^1D), 10^{-3} s^{-1}**	**VOC, ppb**	**OH, 10^7 cm^{-3}**	**HOM, 10^7 cm-3**	**CS, s^{-1}**	**HOM yield, %**	
1	TOF	2.6	5.4	2.2	19.7	$1.7x10^{-3}$	2.5	
2	TOF	3.8	4.6	2.7	21.2	$3.5x10^{-3}$	3	
3	TOF	1.7	7.1	1.4	17	$3.4x10^{-4}$	2.3	
Benzene+NOx								
#	**PTR**	**UV lamp, J(O^1D), 10^{-3} s^{-1}**	**VOC, ppb**	**OH, 10^7 cm^{-3}**	**HOM, 10^7 cm-3**	**CS, s^{-1}**	**HOM yield, %**	**NOx, ppb (NO2:NO)**
1	TOF	2.6	15.4	5.7	-	-	-	4.3 (3:1)
Aerosol seed experiment								
#	**PTR**	**UV lamp, J(O^1D), 10^{-3} s^{-1}**	**VOC, ppb**	**OH, 10^7 cm^{-3}**	**HOM, 10^7 cm-3**	**CS, s^{-1}**	**HOM yield, %**	**SOA yield, %**
1	QMS	2.6	15.7	4.1	7.2	$9.4x10^{-5}$	4.1	40

In this work, we utilize a total of 27 benzene + OH experiments, 3 phenol + OH experiments, 1 benzene + OH + NOx experiment and 1 seed-addition experiment (Table 1). The reaction of benzene and ozone under dark conditions as well as photolysis in absence of ozone were also tested. In these tests, no HOM were detected, and we thus attribute the VOC + OH reaction to be the initiator of all measured HOM in this work. The parameters for each experiment were determined when the chamber had reached steady-state. Typically, each experiment started by adjusting VOC and O_3 concentrations, after which the UV lamp was switched on. Especially at high VOC concentrations, this initiated a strong particle formation event, and it took several hours to reach a steady-state. An example experiment is presented in Fig. 2.

3.2 Instrumentation

3.2.1 CI-APi-TOF

A Chemical Ionisation Atmospheric Pressure interface Time-Of-Flight mass spectrometer (CI-APi-TOF, Jokinen et al., 2012) was used to measure HOM in the Helsinki flow reactor and at JPAC. It consists of a Chemical Ionisation inlet (CI, Airmodus Oy) and an APi-TOF online high resolution mass spectrometer (Junninen et al., 2010, Tofwerk AG/Aerodyne Research Inc.). The CI inlet is designed to minimize wall contact during sampling and utilizes a high sample flow rate of around 10 slpm. Inside the CI inlet, the sample air is co-axially merged with a sheath flow (~20 slpm) of filtered compressed air that contains

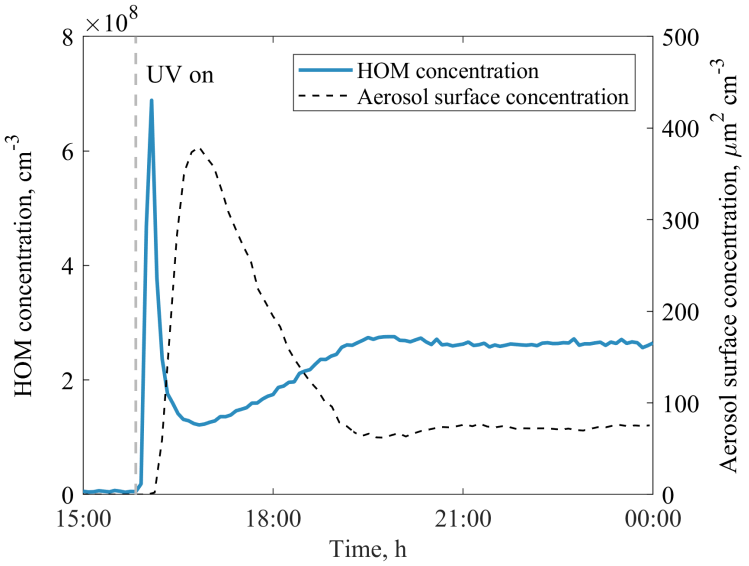

Figure 2. An example of JPAC reaching steady-state after the UV lamp was switched on in experiment #20. Within a few minutes, the concentration of HOM increased significantly triggering particle formation in the chamber, which acted as a sink for HOM. After both the gas- and particle-phase signals reached steady-state (in ~5 hours) the HOM yield was calculated.

nitric acid and nitrate ions. The ions were produced by exposure to either a radioactive source (241 Am α-emitter in JPAC) or soft X-rays (<9.5keV, Hamamatsu L9490 photoionizer in Helsinki flow reactor). Upon collisions with neutral nitric acid, the nitrate ions can form $(HNO_3)_{0\text{-}2}NO_3^-$ adducts, which are referred to as reagent ions. Using an electric field, the reagent ions are pushed into the sample flow and, after ~200 ms of interaction between sample molecules and reagent ions, guided into the APi-TOF through a critical orifice admitting 0.8 l min^{-1}.

If energetically favourable, molecules in the sample air can be ionised via proton transfer or adduct formation. In most cases, the ionization of a molecule M happens as

$$M + (HNO_3)_x \cdot NO_3^- \rightarrow M \cdot NO_3^- + (HNO_3)_x \quad (1)$$

In cases where M is a strong acid, such as sulfuric acid, it may transfer a proton to NO_3^- and be detected in its deprotonated form, but most molecules are detected in clusters with NO_3^-.

Nitrate is strongly bound to neutral nitric acid, and, therefore, ionisation through adduct formation will only happen with molecules that can compete for nitrate against neutral nitric acid (Hyttinen et al., 2015). As a result, the nitrate CI-APi-TOF is selective towards HOM, as they often contain two or more hydrogen bond donors in the form of –OOH (or –OH) groups, and are able to form stable adducts with the nitrate ion (Hyttinen et al., 2015).

Inside the atmospheric pressure interface (APi), sampled ions are guided through two differentially pumped quadrupoles and an ion lens assembly, in which the pressure is gradually decreased. After this, the ions enter the time-of-flight (TOF) chamber, where they are orthogonally extracted, and their flight time to the micro-channel plate (MCP) detector is measured. This flight

time is converted to mass-to-charge ratio (Th) for each ion in data post processing. All data processing, including averaging, mass axis calibration and peak integration, was done using the tofTools software package for MATLAB (Junninen, 2013).

The molecular formulas of sampled ions could be resolved owing to the high resolution (~4000 Th/Th at 125 Th) of the TOF analyser. If an ion was identified to be a HOM, defined here simply as molecules with 6 or more O-atoms (Bianchi et al., 2019), and was the dominant ion (>80% of the signal) at its integer mass, the intensity was determined by integrating over the whole integer mass where this HOM was observed. This approach was concluded to be the most robust method, as an accurate mass axis calibration was at times problematic to achieve, and at the 5-minute time resolution used, peak fitting uncertainties increased due to limited signal-to-noise ratio. By using this type of unit mass resolution (UMR) analysis, we avoided having small variations leading to signals "leaking" into closely lying ions that were also being fitted. While our approach does add uncertainty to the quantification, it is believed to be on the order of 10% (as we limited ourselves to masses where the HOM was the dominant ion). This is much smaller than the uncertainty in the absolute sensitivity calibration of the CI-APi-TOF (see below). In addition, when determining the average HOM intensity for a particular experiment, the background signal, determined before the UV lights were switched on, was subtracted.

The HOM ion count rate was converted to concentration (molecules cm^{-3}) using the following equation (Jokinen et al., 2012):

$$[HOM] = C_f \times \frac{\sum_i HOM_i \cdot NO_3^-}{\sum_{i=0}^{2} (HNO_3)_i \cdot NO_3^-} \quad (2)$$

where $HOM_i \bullet NO_3^-$ is the count rate of individual HOM clusters with NO_3^- and the denominator describes the count rate of the reagent ions. C_f is a calibration coefficient, which in the JPAC experiments in this work was approximated as 1.6×10^{10} molecules cm^{-3} following Ehn et al. (2014), who used gravimetric calibration with perfluoroheptanoic acid (PFHA) for the same setup as used in this study. Ehn et al. (2014) reported the uncertainty of this method as $\pm$ 50%, and we estimate a slightly larger uncertainty here due to the lack of calibrations during our measurement campaign. We estimate an uncertainty in determination of the absolute concentration of $\pm$ 70% with the precision in relative changes of less than 10%.

3.2.2 PTR-QMS and PTR-TOF

VOC and their oxidation products in JPAC were measured by a high-sensitivity Proton-Transfer-Reaction Mass Spectrometer (PTR-QMS, Ionicon Analytik GmbH). The technique is described by Lindinger et al. (1998). Calibrations of the VOC were performed using diffusion sources (Gautrois and Koppmann, 1999). The PTR-QMS operated at 2 minute time resolution and the sampling switched every 20 minutes between the inlet and the outlet of JPAC. The sampling lines consisted of ~10 meter long PFA tubing of 4 mm inner diameter and were heated to 60 °C. The sampling flow rate was 0.5 l min^{-1}. During part of the campaign, a high-resolution PTR-TOF, equipped with a time-of-flight mass spectrometer, was deployed (Graus et al., 2010). The PTR-TOF was calibrated using an advanced Liquid Calibration Unit (LCUa, Ionicon Analytik GmbH) for phenol. Benzene calibrations were performed using a self-made compressed gas standard containing, among other VOC, also 670 ppb of benzene, further diluted using the LCUa. Sampling from the outlet of JPAC was performed via a 2 m long, 1 mm ID PEEK-

sampling line heated to 60°C. In order to cover the VOC measurements during all experiments, the data from both instruments was used, giving preference to the PTR-TOF when it was available.

3.2.3 Aerosol Instrumentation

To measure the particle number size distribution in JPAC a scanning mobility particle sizer (SMPS, electrostatic classifier (TSI 3071) and condensation particle counter (TSI 3025), TSI Inc.) was deployed. The SMPS measured particle concentrations in the size range from 14 to 820 nm in diameter, which were used to calculate the condensation sink (see Sect. 3.4). A high-resolution time-of-flight aerosol mass spectrometer (AMS, DeCarlo et al., 2006; Rubach, 2013, Aerodyne Research Inc.) was used to measure the composition of particles from ~40 nm to 1 μm in diameter in the JPAC. In the AMS, aerosol particles were vaporized at 600 ºC and ionized by electron impact ionization at 70 eV, after which the ions were guided via an ion lens into the time-of-flight mass detector. The AMS was calibrated using ammonium nitrate particles and the concentration of ammonium sulfate and organic aerosol was determined by summing the corresponding fragment ions from the mass spectra. SOA yield was estimated from the AMS as the ratio of produced organic aerosol mass to consumed VOC.

3.3 Determination of OH concentration

In JPAC, the concentration of OH radicals in the experiment was calculated based on the amount of reacted VOC, for which the reaction rate coefficient with OH is known. In the chamber, the concentration of a VOC unreactive to O_3 is represented by the following equation:

$$V \times \frac{d[VOC]}{dt} = F \times ([VOC]_{in} - [VOC]) - V \times k_1 \times [OH] \times [VOC] \quad (3)$$

where the V is the chamber volume, F is the flow rate through the chamber, k_1 is the reaction rate coefficient for OH with the VOC. $[VOC]_{in}$ indicates the average concentration of the precursor compound in the total flow entering the chamber, and [VOC] and [OH] describe the actual concentrations in the chamber, whereby [VOC] is measured at the outflow of the chamber. During steady-state conditions, OH concentration in the chamber can be calculated as follows:

$$[OH] = \frac{1}{t \times k_1} \times \frac{[VOC]_{in} - [VOC]}{[VOC]} \quad (4)$$

where t=V/F is the residence time in the chamber. t was approximately constant throughout the campaign (2900 seconds) and k_1 for 14°C was taken as 1.19×10^{-12} cm^3 s^{-1} for benzene and 3.30×10^{-11} cm^3 s^{-1} for phenol (Bloss et al., 2005; Atkinson and Aschmann, 1989). $[VOC]_{in}$ and [VOC] were both determined by PTR-QMS or PTR-TOF. This method is independent of the instrumental calibration; however, it assumes that benzene is lost solely through the reaction with OH. The determination of [OH] was verified in some experiments by introducing 1,8-cineole in addition to benzene, which confirmed the determined OH concentrations within 6-12%.

3.4 Determination of HOM yield in JPAC

We were able to calculate HOM molar yields from JPAC experiments. For HOM yields in this work, we take a slightly different approach than earlier studies where the yield has directly been equated with a branching ratio of a certain VOC-oxidant reaction. We define the molar yield γ of HOM as the fraction of reacted VOC that produced HOM during the residence time in our chamber. This definition includes also HOM formation from molecules reacting multiple times with OH, i.e. multi-generation OH oxidation. We take this approach since the oxidation products will react with OH much more rapidly than the parent VOC benzene, which subsequently means that the primary fate of the first generation oxidation products of benzene will be to undergo further OH reactions. In other words, the more atmospherically relevant quantity, for instance relating to SOA formation, is the ultimate amount of HOM formed, rather than only the HOM branching ratio in the initial OH reaction. The change in HOM concentration in time is defined as HOM production rate minus HOM loss rate:

$$\frac{d[HOM]}{dt} = Production_{HOM} - Loss_{HOM} = k_1\gamma[VOC][OH] - k_{loss}[HOM]$$

where k_1 is the ~~benzene-OH~~ VOC-OH reaction rate coefficient as described in section 3.3, γ is a HOM molar yield, and ~~kloss~~ k_{loss} is the total loss coefficient of HOM to the chamber walls (k_{wall}) and to aerosol particles present in the chamber (i.e. the condensation sink, CS)~~.~~:

$$k_{loss} = k_{wall} + CS$$

Here we assume that HOM are low-volatile enough that these are the dominant loss pathways, and that flushout from the chamber, at a rate of 1/48 min^{-1}, can be ignored. We again stress that γ is not only the branching ratio for the initial VOC+OH reaction, but the fraction of reacted VOC molecules that become converted into HOM in the chamber, irrespective of detailed formation pathways. In steady state in JPAC, the concentration of HOM is constant, so

$$\frac{d[HOM]}{dt} = 0$$

and, therefore

$$k_1\gamma[VOC][OH] = k_{loss}[HOM]$$

Then, the molar HOM yield can be calculated as

$$\gamma = \frac{k_{loss}[HOM]}{k_1\gamma[VOC][OH]} \frac{k_{loss}[HOM]}{k_1\,[VOC][OH]} \quad (5)$$

For k_{loss}, we needed to assume that HOM condense irreversibly, which is a valid assumption based on earlier studies (e.g., Ehn et al., 2014). In accordance with Ehn et al. (2014), and verified in our experiments (not shown), ~~kwall~~ k_{wall} of 0.011 s^{-1} was used. Average HOM concentrations for runs were calculated as a sum of all identified peaks with an oxygen content more or equal to six atoms. In case of phenol experiments, the peaks of the same composition were used as in benzene experiments

for better comparison. The condensation sink was calculated using the following equation (Kulmala et al., 2012).

$$CS = 2\pi D \sum_{d_p} \beta_{m,d_p} d_{d_p} N_{d_p} \quad (6)$$

where D is the diffusion coefficient for condensing vapour ~~(determined by the molecular mass of each HOM)~~ and $\beta_{m,\,dp}$ is the correction factor for the transition regime calculated based on the Fuchs-Sutugin approximation. D was approximated as 0.06 $cm^2\ s^{-1}$ based on the mean molar mass 237 g mol^{-1} and approximated diffusion volume 170 of the observed HOM, according to the approach described by Fuller et al. (1966). d_p is the diameter of particle size bins, and N_{dp} is the concentration of particles in the chamber in the size bin d_p.

Finally, we stress that the HOM yield depends on our ability to determine the HOM concentrations, and is thus associated with at least the same ± 70% uncertainty. Additional uncertainty will arise from the other parameters in Eq. (5), but these are likely to be much smaller than the uncertainty arising from HOM quantification. As stated earlier, only clearly identifiable peaks were utilized for HOM concentration calculations, in order to make the quantification as robust as possible. ~~This means that we likely missed some HOM signal in the many smaller peaks that were unidentified or in the omitted peaks that showed contaminants at the same unit mass . Thus~~These peaks constituted approximately 50% of the total signal in mass range from m/z 200 to 550. Although isotopes account for some of this unexplained fraction, our approach may cause an underestimation of the HOM yields by up to 50%.

3.5 Chamber kinetic model

In order to model HOM condensation during the seed addition in JPAC, we have constructed a simple kinetic model. The HOM mass concentration was modelled with 0.1 s resolution and the model assumed that the chamber was perfectly mixed for every time point. HOM molecular concentration for each point in time j for each HOM molecule i was calculated by adding the HOM produced in a cm^3 in 0.1 s and subtracting the HOM lost from the HOM concentration in previous time point (j-1) as follows:

$$\begin{aligned}[HOM]_{j,i} &= [HOM]_{j-1,i} + 0.1s \times (Production_{HOM} - Loss_{HOM}) \\ &= [HOM]_{j-1,i} + 0.1s \times (\gamma k_1 [OH]_{j-1} [VOC]_{j-1} - k_{loss} [HOM]_{j-1,i}) \end{aligned} \quad (7)$$

~~HOM molar yield γ was set at~~ The molar yield of total HOM was set to 5% to ~~reproduce the initial~~ match the measured HOM concentration ~~.~~before seed addition. For an individual HOM_i, the relative abundance in the spectra determined its yield. [VOC] was set to constant 15.7 ppb (as measured by PTR-QMS), while [OH] concentration was scaled to match start and end measured HOM concentration (see Sect. 4.2.4). In Eq. (7), k_{loss} took into account both wall loss and CS. The loss of HOM due to the flush out from the chamber was excluded as it is negligible compared to wall loss and CS in JPAC. Then, the total HOM mass concentration at point in time j equaled

$$[HOM\ mass]_i = \sum_{i=1}^{n} [HOM\ mass]_{j,i} = \sum_{i=1}^{n} \frac{[HOM]_{j-1,i} \times M_i}{N_A} \quad (8)$$

where M_i is the molar mass of HOM molecule i and N_A is Avogadro's constant. If a HOM molecule was detected as cluster with NO_3^-, M_i was calculated as the m/z value of the peak minus the mass of NO_3^-. For this model, we used the peaks corresponding to the same HOM molecules as in the HOM yield calculation, 69 peaks in total. The list of the m/z values and corresponding compositions can be found in Table S4 in Supplement.

4 Results and Discussion

4.1 Flow reactor study

In the first part of this work, we studied the OH oxidation of benzene, toluene and naphthalene in the Helsinki flow reactor using a nitrate-based CI-APi-TOF. In all three systems, we observed the formation of highly oxygenated organic molecules (HOM). Product distributions are shown in Fig. 3 and include both HOM (products with six or more O-atoms) and less oxidized species, which were detected as adducts with NO_3^-. The following discussion focuses on peaks detected by adduct formation. We omit the reagent ion NO_3^- when presenting the molecular formulas. However, the mass of the molecules refer to the correct mass, including the nitrate ion.

A few prominent peaks clearly dominated the benzene spectrum (Fig. 3a) with oxygen content of the products ranging from 4 to 13 atoms. Among the closed-shell HOM, $C_5H_6O_7$, $C_5H_6O_8$, $C_6H_8O_8$, $C_6H_8O_9$, $C_6H_8O_{11}$ monomers and $C_{12}H_{14}O_8$, $C_{12}H_{14}O_{10}$, $C_{12}H_{14}O_{12}$, $C_{12}H_{14}O_{14}$ dimers dominated the signal. Also two radicals, $C_6H_7O_9$• and $C_6H_7O_{11}$•, were detected.

The bicyclic peroxy radical (BPR), $C_6H_7O_5$• in the case of benzene, is potentially an intermediate in the formation of many HOM in the oxidation of aromatics. It was proposed in earlier studies that BPR from substituted aromatics can undergo further autoxidation (Molteni et al., 2018; Wang et al., 2017). In the case of benzene, it would form radicals with chemical composition $C_6H_7O_x$• , where x is an odd number larger than five. This hypothesis is supported by the presence of $C_6H_7O_9$• and $C_6H_7O_{11}$• radicals, while BPR itself and the $C_6H_7O_7$• radical are detected only as very small signals. This is most likely due to the reduced detection efficiency for smaller radicals. While BPR is expected to have only one OH-group and its detection is unlikely, the reason for the low abundance of $C_6H_7O_7$• in the spectrum is unclear. It would be explained, however, if $C_6H_7O_7$• would contain two endoperoxides and a peroxy group, as also proposed by Molteni et al. (2018), therefore, still having only one OH group to supply a hydrogen bond to a nitrate ion.

While $C_6H_7O_5$• (BPR) is weakly detected as such, we can observe products consistent with its termination reactions. For instance, $C_6H_8O_5$ at 222 Th can be formed through BPR reacting with HO_2. In photo-oxidation of any VOC, HO_2 production from RO_2 is efficient. HO_2 ~~can also be produced~~ will also be co-produced from water photolysis in our reactor making a reaction with HO_2 an important bimolecular termination pathway~~in our system~~. This is also supported by the observation of $C_6H_8O_7$, $C_6H_8O_9$, $C_6H_8O_{11}$ and $C_6H_8O_{13}$. However, high oxygen content of HOM as well as the existence of dimeric species shows that the termination of RO_2 by HO_2 was not a dominant process in our system

The other important termination agents in our system are RO_2 radicals. The dominance of the $C_{12}H_{14}O_8$ dimer in the spectrum, likely formed from BPR self-reaction, strongly indicates the importance of ROOR' dimer formation. The prominence of dimers with even oxygen numbers (also $C_{12}H_{14}O_{10}$, $C_{12}H_{14}O_{12}$, and $C_{12}H_{14}O_{14}$) is consistent with primarily odd-oxygen

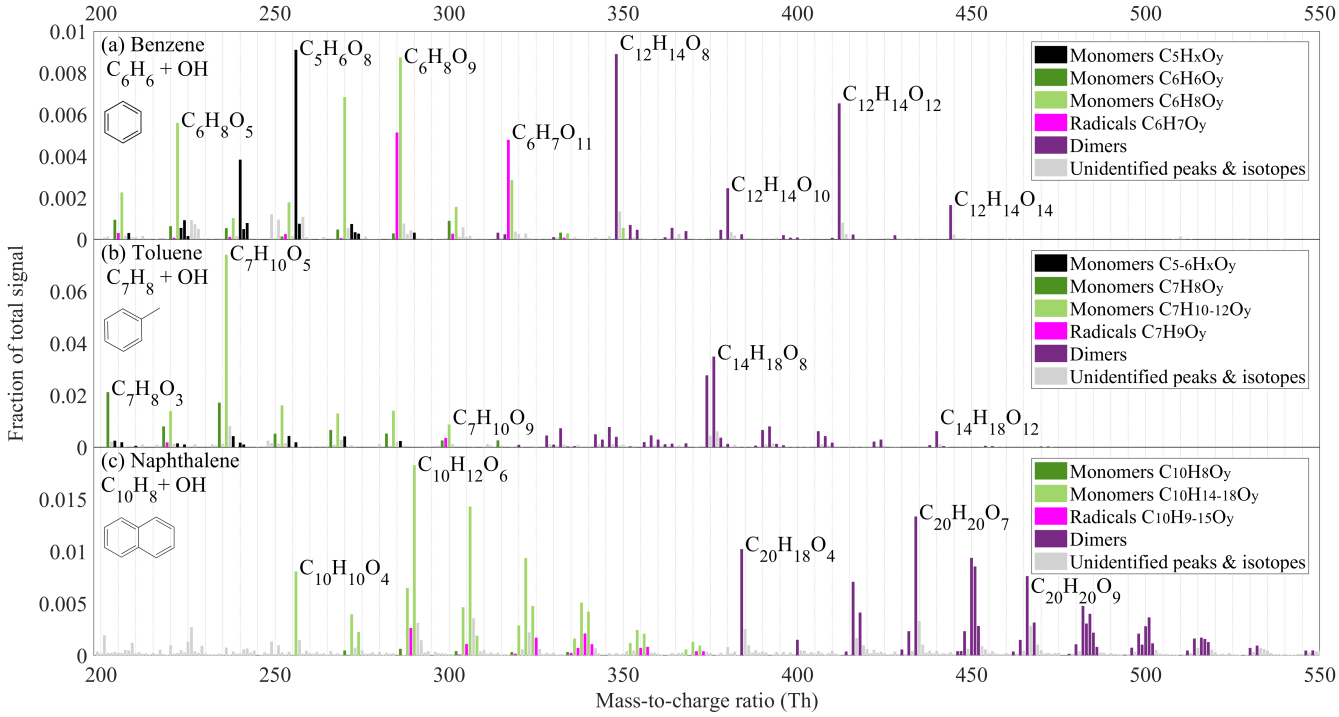

Figure 3. Spectra of organic oxidation products observed in oxidation of a) benzene, b) toluene and c) naphthalene. The y-axis shows the signal normalized by the total ion count of the instrument. The colours indicate different compound groups, as described in the legend of each subplot. The unit masses with more than one peak are marked with the colour of the most abundant peak. All the peaks above 200 Th are detected as adducts with NO_3^-, which is excluded from the labels. The full list of peaks can be found in Supplement (Tables S1-S3). Unidentified masses, isotopes and contaminant peaks are marked in light grey.

RO_2 being formed in the benzene system. If even-oxygen RO_2 were also abundant, odd-oxygen dimers, from cross reactions of odd- and even-oxygen RO_2, should be more prominent in the spectrum.

Monomer HOM with even number of O-atoms are also abundant in Fig. 3a, and these can be formed from RO_2 cross-reactions forming a carbonyl and an alcohol, or via alkoxy (RO) radical pathways. We are not able to separate formation pathways in such detail based on our data. However, the importance of RO radicals is suggested by some C5 radicals that we observed, namely $C_5H_7O_6$•, $C_5H_7O_8$•, and $C_5H_7O_9$•, with one carbon less than benzene. Since benzene is a plain aromatic ring, loss of carbon from this molecule is only possible after a ring opening, potentially due to RO decomposition or another reaction causing the break of a bond between carbon atoms. After the ring is broken, CO or CO_2 could be lost and, after a reaction with another O_2, $C_5H_7O_x$• radicals are formed. These RO_2 radicals would terminate by reacting with HO_2 or another RO_2. Indeed, C_{10} and C_{11} dimers as well as closed-shell C_5 products are observed, of which $C_5H_6O_8$ (256 Th) is one of the

dominant peaks in Fig. 3a. We cannot rule out other pathways for loss of carbon atoms from the molecules, and only conclude that it is a non-negligible pathway for HOM formation in benzene oxidation under our conditions.

The product spectrum from our flow reactor study of benzene oxidation shown in Fig. 3a was similar to the previous study by Molteni et al. (2018). For instance, the three largest signals in their study above 200 Th were $C_6H_8O_5$, $C_5H_6O_8$, and $C_{12}H_{14}O_8$, which are also prominent signals in our spectrum. Overall, almost the same molecules are present, with some variations in relative abundance. Specific differences worth noting are the larger fractions of RO_2 radicals visible in our spectrum, with two radicals ($C_6H_7O_9$• and $C_6H_7O_{11}$•) being among the highest peaks. In contrast to our experiment, Molteni et al. (2018) observed dimers with odd and even amount of oxygen at comparable concentrations, suggesting the presence of both even- and odd-oxygen radicals in their system. While the specific experimental conditions between the studies of Molteni et al. (2018) and ours were not identical (benzene concentration ~100 times higher, residence time 50 % shorter, UV lamp irradiating part of the flow reactor in our study), some differences in the spectra are expected. However, based on the good agreement in product composition between the two studies, we conclude that direct photolysis of the VOC or its oxidation products (whether radicals or closed-shell species) were not affecting our results to a large extent. In addition, in our flow reactor, a direct photolysis experiment in absence of water showed no HOM formation. Nevertheless, future studies are needed to determine the exact role of photolysis in comparison to OH oxidation in initiating HOM formation in such systems.

In our flow reactor, we also tested the oxidation of toluene (C_7H_8, Fig. 3b). While the composition of toluene oxidation products generally is consistent with the reactions described for the benzene system above, some notable differences are observed. For instance, compared to the benzene experiment, the signal spreads out more evenly over many ions in the monomer product mass range, except for the dominant $C_7H_{10}O_5$ peak. Analogously to the benzene system, this is likely a termination product of a BPR in reaction with HO_2. Another difference is that even-oxygen dimers do not dominate the dimer spectrum. Instead, only two peaks, $C_{14}H_{18}O_8$ and $C_{14}H_{16}O_8$ are dominant. While the former dimer could originate from toluene-BPR self-reaction, the origin of the latter is unclear. We also observed some monomers with five or six carbon atoms, though at much lower contribution to total than the contribution of C_5 monomers in the benzene experiment. Overall, in comparison to the study by Molteni et al. (2018), where the toluene concentration was about 25 times smaller than in our experiments, many of the peaks are similar. Specifically, it is interesting that in the toluene system, we also observed a few $C_7H_{12}O_{4\text{-}8}$ products with four hydrogen atoms more than in toluene itself, indicating the potential secondary OH oxidation (addition) step (Molteni et al., 2018). These products overlapped with $C_6H_8O_x$ compounds in the spectrum, so while they can be separated in high-resolution analysis, they are not recognisable in Fig. 3b.

In our naphthalene ($C_{10}H_8$) experiment, which is presented in Fig. 3c, the signal was distributed among an even larger amount of product peaks than in the toluene experiment. Interestingly, the largest monomer ($C_{10}H_{12}O_6$) contained 4 H-atoms more than the naphthalene precursor ($C_{10}H_8$). This suggests that an oxidation pathway including two OH attacks in combination with two HO_2-termination reactions was important in the naphthalene system. Evidence of RO_2 radicals formed through two OH attacks is also seen in H_{20} dimers, which likely formed through cross-reaction of H_9 and H_{11} RO_2. In the benzene spectrum we did not observe any monomers containing four hydrogens more than the parent VOC, while in the toluene spectrum we observed only a minor fraction of such peaks. We attribute this to the higher VOC concentration used in our benzene experiment (400 ppm),

in comparison to naphthalene (0.4 ppm) and toluene (25 ppm). The OH production from H_2O photolysis stayed constant in our experiments, but the VOC acts as a sink for the OH radicals, which means that higher VOC concentrations will result in lower OH concentrations. This, in turn, decreases the likelihood of oxidation products reacting with OH a second time in our flow reactor. Therefore, not only the competition between autoxidation and bimolecular RO_2 termination reactions will govern the exact concentration and distribution of HOM, but also the amount of secondary (or higher) OH attacks. For determining the importance of multi-generation OH oxidation as a source of HOM, longer time scales and lower VOC concentrations than reachable in our flow reactor were needed. Our further investigations in the JPAC chamber facility at the Research Centre Jülich were well suited for such a task.

4.2 JPAC chamber studies

4.2.1 HOM yields

To continue our study on the formation of HOM from aromatics, we performed systematic studies of benzene oxidation in the JPAC chamber (see Table 1). In JPAC, we were able to control the experimental conditions in more detail than in our flow reactor. In experiments without NO_X, the main parameters determining the oxidation process were the concentrations of OH and VOC. As described in Sect. 3.1.2, these two parameters could be adjusted by changing the inflow of VOC or ozone, or by adjusting the photolysis rate by changing the gap width of the UV filter. Out of these, the input of VOC had the largest range, spanning around two orders of magnitude (1.6-112 ppb). An increase of VOC also meant a larger sink for OH, and thus the VOC and OH concentrations in the chamber were codependent.

Figure 4a shows the measured HOM concentrations as a function of the VOC oxidation rate ($k_1 \times [VOC] \times [OH]$), including primarily benzene experiments (square markers) but also three phenol experiments (circles). ~~At~~ In benzene experiments at small oxidation rates, the total HOM concentration increased linearly, but ~~reached a plateau around 3-4~~ a plateau at around 3×10^8 cm^{-3} was visible at higher oxidation rate. If the loss coefficient (k_{loss}) of HOM were constant throughout all runs, experiments with the same HOM yield would fall on the same line. Assuming the loss of HOM is only determined by wall loss ($k_{loss} = k_{wall}$), the plotted lines in Fig. 4a would correspond to 2.5, 5 and 10% yields. However, especially in the high [VOC] experiments (markers on the right hand side of Fig. 4a), the CS due to particles formed in the chamber was of the same order as the wall loss and thus the approximation that k_{loss} equals k_{wall} is not valid anymore. In addition, the high-OH experiments (dark blue points) seem to result in the highest HOM yields.

In order to identify the role of OH concentration for HOM yields, we calculated the molar yields, i.e. the number of HOM molecules formed per reacted precursor VOC molecule, according to Eq. (5), properly accounting also for the CS. The results are shown in Fig. 4b. It is clear that under the conditions probed in JPAC, the main determining factor for the HOM yield was the OH concentration. ~~The OH concentration in the chamber was clearly higher than in the atmosphere, but the average reaction time in the chamber was limited to approximately 48 minutes. If utilizing the concept of equivalent OH dose, a 48-minute residence time with OH = 10^7 – 5×10^8 cm^{-3} is equivalent to atmospheric oxidation times of roughly 10 h – 15 days at OH concentration of 10^6 cm^{-3}. In other words, our experiments span a reasonable range of atmospheric lifetimes~~It should be noted

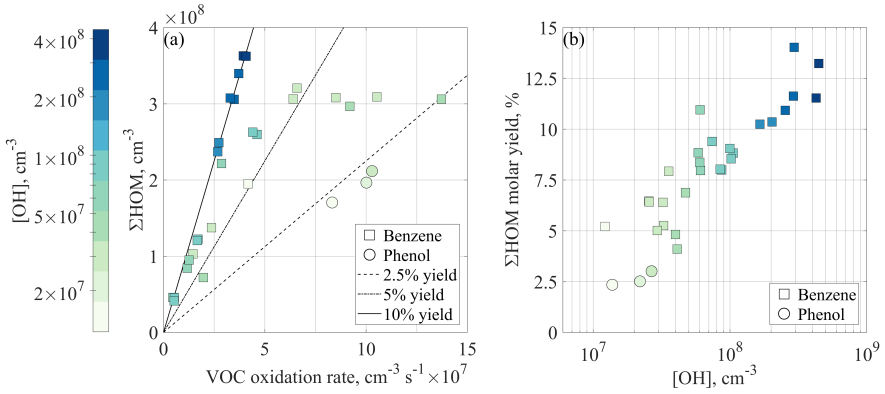

Figure 4. HOM concentrations and yields observed in the JPAC experiments. a) Total HOM concentration plotted as a function of VOC oxidation rate. If the HOM loss rate is constant between the experiments, conditions with the same molar HOM yields should fall on the same lines. The included lines (for 2.5, 5, and 10% yields, respectively) neglect the condensational sink (CS) and depict the yields in the case where loss to walls is the only sink for HOM. The color represents the concentration of hydroxyl radicals, squares depict benzene runs, while circles show phenol runs. b) Calculated HOM molar yields as a function of OH concentration in the chamber corrected for CS. Markers are the same as in panel a, as is the color code for easier comparison.

that the specific dependency of HOM yield on OH may vary if other gases and loss mechanisms would be present. Since the observed HOM molar yield increased, we can conclude that the undetected lower oxygenated products reacted again with OH to form more of the detectable HOM. These intermediate precursors could also be higher oxygenated compounds that were detected in our instrument with ionisation efficiency below the collision limit (Hyttinen et al., 2015).

Our estimated HOM yields from benzene oxidation were 4.1-14.0%, which can be compared to a value of 0.2% provided by Molteni et al. (2018). ~~Their value~~ The difference in the results is expected due to the substantial difference in the studied timescales (20 second in their study). In addition, in their flow reactor, air parcel was exposed to an initial OH concentration that decreased as OH reacted away, while in JPAC, the OH was produced continuously. This resulted in different OH doses in the systems. Considering these differences, less oxidation steps would be expected in a flow reactor. As a result, the yield in Molteni et al. (2018) likely corresponds to the HOM yield of the first OH oxidation step, potentially also impacted by a second step~~, suggesting~~ . This suggests that more than 90% of the "HOM- forming potential" of benzene comes from multi-generation OH oxidation in combination with slower isomerization reactions that may not be observed on shorter time scales.

To test secondary OH oxidation, we conducted three similar experiments starting with phenol as the precursor, a known first-generation oxidation product of benzene. ~~In order to test the importance of the phenol pathway in HOM formation, three experiments were conducted solely with phenol .~~ Examining Fig. 4b, the phenol experiments show the lowest HOM yields (2.3 – 3%), suggesting that the phenol oxidation pathway is not the major route to form ~~multi-generation~~ HOM from benzene. However, the phenol experiments do not fall far from the trend produced by the benzene experiments, and thus phenol is likely to contribute to the total HOM formation from benzene. The OH concentration in the chamber was clearly higher than in the

atmosphere, but the average reaction time in the chamber was limited to approximately 48 minutes. If utilizing the concept of equivalent OH dose, a 48-minute residence time with [OH] = 10^7 – 5×10^8 cm^{-3} is equivalent to atmospheric oxidation times of roughly 10 h – 15 days at OH concentration of 10^6 cm^{-3}. In other words, our experiments span a reasonable range of atmospheric lifetimes.

In comparison to biogenic VOC, our results were closest to the HOM yields observed in ozonolysis of α-pinene and limonene, 3.4-7% and 17% respectively (Bianchi et al., 2019). In the biogenic systems, especially if a VOC contains an endocyclic double bond, the first oxidation step by O_3 is known to form HOM at large yields. On the other hand, the observed yields in first-step OH oxidation are reported to be low (~1%, (Bianchi et al., 2019)). To our knowledge, no studies exist that explore HOM yields of biogenic VOC oxidation as a function of OH concentration. However, McFiggans et al. (2019) indicated a non-linear increase of HOM concentration with increasing α-pinene oxidation rate. We would therefore expect that also in biogenic systems, an increase in HOM yield due to multi-generation OH oxidation could be observed.

4.2.2 Variability in HOM spectra

In addition to total HOM yield, OH concentration also affected the distribution of monomers and dimers in the benzene HOM spectrum, which is seen in Fig. 5 a-b. Higher OH concentration produced a spectrum with more peaks than did lower OH, indeed pointing at multiple oxidation steps. At lower OH, the monomers somewhat resembled the benzene flow reactor experiment. In Fig. 5a and b, the VOC oxidation rate is very similar (4.2×10^7 versus 3.9×10^7 cm^{-3} s^{-1}), while OH concentration is 35 times larger in Fig. 5b (4.5×10^8 versus 1.2×10^7 cm^{-3}). The HOM yields corresponding to Fig. 5a and to Fig. 5b are 5.2% and 13.2%, respectively.

As OH increased in benzene experiments, an increase in the abundance of products with more H-atoms than the parent molecule due to secondary OH addition was expected; however, we observed an increase in products with lower H content, H = 4-6. This means that OH oxidation through H-abstraction started to play a role. Oxidation of benzoquinone (formed in OH oxidation of phenol, MCM3.3.1 Bloss et al., 2005) could also potentially explain $H_{4\text{-}6}$ monomer HOM. After ring-opening, the BPR will contain one double bond, and if the products retain this, one more OH addition is possible. However, after this, OH oxidation can only proceed via H-abstraction, and if the subsequent termination reactions occur by loss of OH or HO_2, a decrease in H-atoms will take place. In other words, it is to be expected, that multi-generation OH oxidation will produce also molecules with less H-atoms than the parent VOC.

The dimers detected in JPAC experiments had up to 18 oxygen atoms, which was larger than seen in flow reactor study. Dimers in JPAC had larger variability in the H-atom content, from 10 to 16. As in monomers, the dimer distribution also varied with OH concentration. At higher OH concentrations, a larger fraction of dimers was C_{11} dimers suggesting more efficient formation of C_5 radicals. At lower OH concentrations, the dimer distribution ~~partly resembled~~ was more similar to the distribution seen in the flow reactor~~, while at higher OH, the dimer spectrum was distributed over a large number of peaks~~. In addition, in JPAC, the dimer-to-monomer ratio was observed to decrease with increased OH concentration. This may be explained by higher HO_2 concentrations at higher OH. Another ~~possibility is that the dimer formation upon RO_2 +R'O~~possible explanation is that RO_2 ~~reaction would be less likely for the RO_2 formed at high OH~~ formed at higher OH would have less

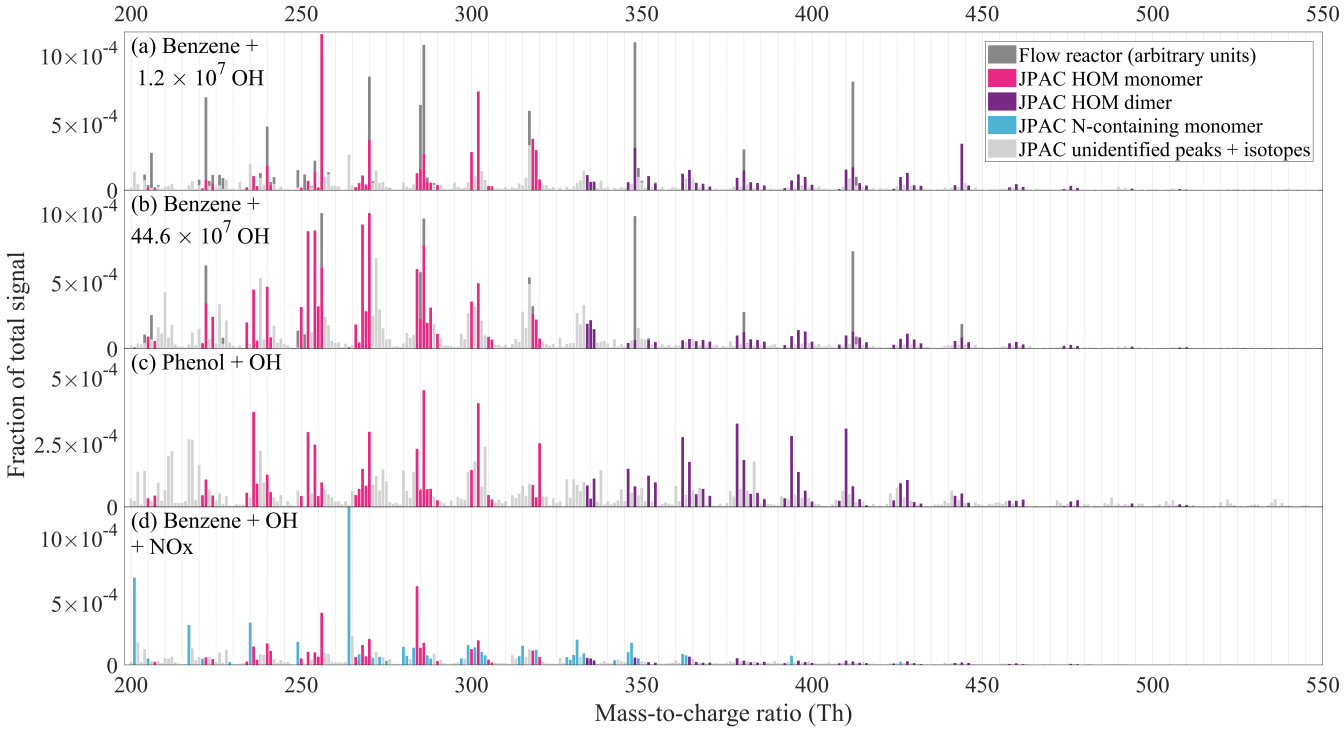

Figure 5. CI-APi-TOF spectra observed during experiments at JPAC. The y-axis shows the signal normalized to total ion counts. Panel a shows the mass spectrum of benzene oxidation at the lowest OH concentration among our experiments, while panel b corresponds to the highest OH concentration. In panel a and b, the scaled flow reactor mass spectrum is also included for comparison (dark grey bars, in arbitrary units). Panel c shows the oxidation products of a phenol oxidation experiment. In a, b and c, the colour schemes are identical and non-grey peaks represent those that were included in HOM yield calculation, with exception of few peaks. The full list of peaks is presented in Supplement (Table S4). Panel d shows the benzene + OH experiment in presence of NO_X, where N-containing ions ("N-containing monomers") dominate the spectrum.

favourable structures for dimer formation. The dimer formation rate has been shown to be highly dependent on the structure of the reacting RO_2 ~~(Berndt et al., 2018b)~~(Berndt et al., 2018a).

In the phenol experiments (Fig. 5c), most elemental compositions were similar to those starting with benzene, as could be expected given that phenol has the same amount of C- and H-atoms as benzene. However, the relative distribution of peaks in the phenol spectrum did not directly resemble either the low or the high OH concentration benzene spectrum, again suggesting that a considerable fraction of HOM were produced from non-phenol pathways. In Fig. 5c, the peaks in colour are the same peaks as were observed in the benzene experiments and were used for HOM yield calculations. Compared to the benzene experiments, phenol produced more dimers, of which H_{12} dimers were a significant fraction, suggesting that H_5

radical production in phenol oxidation was somewhat more important than in benzene oxidation (H_5 and H_7 radicals would react to form H_{12} dimers).

4.2.3 NO_X experiment

While not being the main focus of this study, we also added NO_X to the chamber in order to see its effect on HOM formation from benzene. Aromatic VOC and NO_X are often co-emitted, and thus our no-NO_X experiments are mainly relevant in places where the emissions were sufficiently diluted following transport from the vicinity of the sources. As seen in Fig. 5d, we observed many nitrogen-containing HOM as well as less oxidized compounds likely relating to nitrophenol-type compounds (i.e., nitrophenol with additional -OH or -NO_2 groups). The list of observed products is presented in Supplement (Table S4). In addition, we observed also HOM without nitrogen, presumably from the reaction pathways involving alkoxy radicals (formed from RO_2+NO).

The nitrophenol-type compounds reacted much slower to changes in the chamber compared to HOM, likely indicating condensation and re-evaporation from chamber walls (i.e. semi-volatile compounds). As such, they can likely be transported long distances in the atmosphere, as shown in a recent study, which found a large nitrophenol signal in a CI-APi-TOF in the boreal forest (Yan et al., 2016). This study also showed that nitrophenol, despite only having one OH group, is readily detected by the CI-APi-TOF. Hyttinen et al. (2017) confirmed the stability of nitrophenol clusters with a nitrate ion using quantum chemical calculations.

4.2.4 HOM contribution to SOA

To examine the role of the observed HOM on SOA formation, we added ammonium sulfate seed aerosol to the chamber during one experiment. Aerosol addition increased the condensational sink for low-volatility species in the chamber. Many of these compounds would otherwise condense onto the chamber walls. Upon addition of the seed aerosol, HOM concentrations decreased and SOA concentrations increased (Fig. 6). Ehn et al. (2014) observed a similar behavior in JPAC experiments during ozonolysis of α-pinene. In the Ehn et al. (2014) experiments, the ~~condensed HOM explained more than 50% of the formed SOA mass at~~ total aerosol mass loading was 30 μg m^{-3}~~total mass loading, including~~ , out of which 7 μg m^{-3} ~~organics, while in our case the removed HOM explained around 30% at the highest total~~ was the SOA mass formed during the experiment. The condensed HOM explained more than 50% of that SOA mass. In our benzene case, at total aerosol mass loading of 22 μg m^{-3}, ~~which contained~~ the removed HOM explained around 30% of the 2.7 μg m^{-3} SOA mass. The chamber did not fully reach steady-state before the seed addition, which adds some uncertainty to the estimates, as discussed in the next paragraph. We expect that addition of seed aerosol will not affect the VOC oxidation rate, therefore VOC mass reacted should be the same over the whole experiment. Since the SOA yield is defined as SOA mass formed over VOC mass reacted, the observed increase of SOA directly indicates an increased SOA yield. In our case, the calculated SOA yield was ~~neglible~~ negligible before seed addition, and increased to about 40% at the peak aerosol concentration of 22 μg m^{-3}. This clearly suggests that aerosol loadings can greatly influence SOA yield estimates from chamber studies as long as wall loss can compete with CS (Ehn et al., 2014; Kokkola et al., 2014; Zhang et al., 2014). We acknowledge that most SOA yield studies have been performed

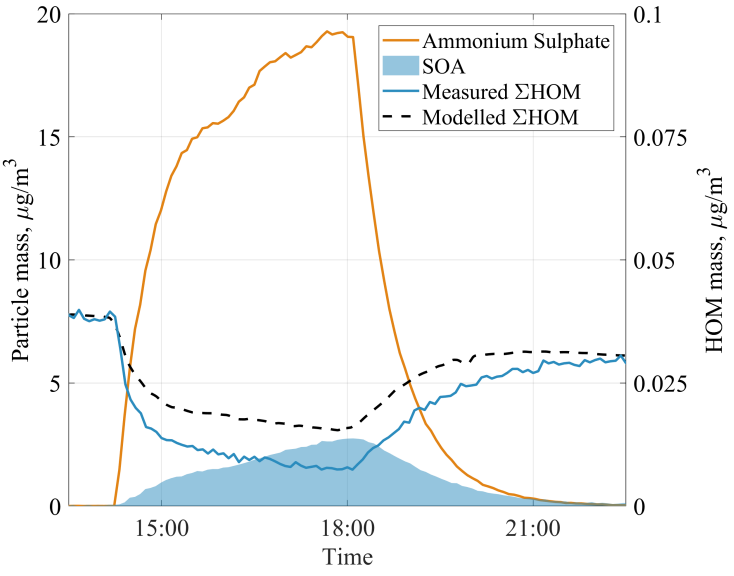

Figure 6. The evolution of components of aerosol mass and HOM mass concentrations during a seed aerosol experiment. The modelled total HOM concentration (dashed line) underestimates the removal of HOM from the chamber when aerosol seed is added, suggesting that not only HOM, but also some HOM precursors, decrease during the seed addition.

in larger chambers where the wall loss rate can be much smaller than in our chamber, and thus the effect is unlikely to be quite as large as observed here. The final SOA yield of 40% in our study is similar to 37% yield in a low-NO_X regime reported in previous work (Ng et al., 2007).

We constructed a simple chamber model to test the expected loss of HOM at different seed loadings, matching HOM concentrations to the periods before and after seed addition. HOM loss rates are a sum of wall loss rate (estimated as 0.011 s^{-1}) and condensational sink, which is calculated for every point in time according to Eq. (6), using the measured aerosol number size distribution. It should be noted that condensation sink assumes that the vapour is non-volatile. The reason behind the HOM concentration not returning to the same level as before seed addition (~25% lower at the end of the experiment) is unclear. VOC in and outflow were stable, as were ~~O_3~~ O_3 concentration and RH. As consequence, OH was also constant within the error ranges with a tendency to drop by about 10% over the time when seed aerosol was present. In our model we included a linear decrease of the OH concentration over the experiments to match the start and end HOM concentrations.

Using our model, we capture the shape of the HOM decrease very well, but find that our model underpredicts the loss of HOM to the particles (Fig. 6). A possible explanation is that we underestimate the condensation sink (CS) or overestimate the wall loss rate (k_{wall}) in our model. For k_{wall}, the value would need to be ~2.5 times lower, corresponding to an inverse lifetime of 220 s, which is not supported by earlier experiments (Ehn et al., 2014) and observed lifetimes of individual HOM in our experiments. A similar correction factor of ~2.5 would be required for the CS in order to match the measurements, and this is

a much greater value than the uncertainty in the aerosol loading data used for the CS calculation. In addition, the discrepancy is larger for some of the detected HOM, while for others the model matches the observed loss (Fig. A1, A2 in Appendix A).

The most likely explanation for the mismatch in Fig. 6, Fig. A1, and Fig. A2, is that by introducing the seed aerosol we introduce a sink not only for the HOM detected by the CI-APi-TOF, but also for some ~~precursors for multi-generation HOM formation that are undetected by our instrument~~ of the undetected oxidation products (or detected at ~~lower sensitivity~~)low sensitivity), that could have formed detectable HOM upon further OH oxidation steps. This explanation is plausible and is in support of our hypothesis that some of the HOM were formed in multi-generation ~~HOM hypothesis~~ OH oxidation. It also suggests that both the detected benzene-derived HOM and some of the HOM precursors are sufficiently low-volatile to condense on 100 nm seed aerosol. If a HOM molecule were not to condense irreversibly onto the aerosol surface, it would lead to the opposite effect, i.e. that our model would overpredict the loss of HOM due to seed addition. Based on the explanation above, we note that our earlier estimate of HOM contribution to benzene SOA of 30% is a slight overestimation. Based on our current understanding of HOM and the results from our SOA experiment, we expect that the change of HOM yield with OH would affect in turn the formed SOA yield. It is likely, that this effect will be mainly pronounced in SOA studies conducted without seed aerosol or in studies where seed aerosol is added at low concentrations (Ehn et al., 2014).

5 Summary and Conclusions

In this study, we confirmed the production of highly oxygenated organic molecules (HOM) in the OH-induced oxidation of aromatic compounds. We tested this chemical system in a flow reactor (10-second residence time) and in the Jülich Plant Atmosphere Chamber (JPAC; 48-minute residence time).

In benzene oxidation experiments in the flow reactor, we most likely observed first-generation HOM formed after a single OH attack. In experiments of toluene and naphthalene, we observed a broader distribution of HOM molecules, within which no particular compound clearly dominated the signal. We attributed this difference to lower VOC concentrations in the toluene and naphthalene systems compared to the benzene system, resulting in higher OH concentrations and consequent multiple OH reactions.

Complementary to the flow reactor study, we further investigated the multi-generation OH oxidation as a source for HOM in JPAC, specifically focusing on quantifying the benzene-derived HOM yield. The HOM molar yield, which in our definition included also multi-generation oxidation, in JPAC varied from 4.1 to 14.0% and strongly depended on the OH concentration. This dependence suggested that multi-generation oxidation produced a major portion of HOM. When examining the HOM composition, higher OH concentrations caused a larger variety in HOM products, with H-abstraction oxidation becoming more significant. We also noted a decrease in the dimer-to-monomer ratio as OH increased.

In a phenol oxidation experiment (a first-generation product of the benzene reaction with OH), we observed a lower HOM molar yield in comparison to the benzene oxidation at a comparable VOC oxidation rate and OH concentration. The lower HOM yield in phenol oxidation suggests that the non-phenolic pathway must be significant for HOM formation from benzene. This was further supported by the difference of the spectral distribution of HOM products between phenol and benzene.

Upon addition of about 4 ppb NO_X to the benzene system in JPAC, we observed a production of N-containing HOM. These likely contained both nitrate- and nitro- functionalities. While termination reactions by NO_X were significant, many HOM without nitrogen were still observed. The HOM spectrum observed in this experiment likely is more representative of the ambient urban air, where NO_X concentrations are high. On the other hand, experiments without NO_X are representative of the emissions after considerable dilution.

We also tested the ability of HOM from benzene oxidation to form secondary organic aerosol (SOA). We introduced seed aerosol to JPAC and investigated the rate of condensation of HOM. The loss of HOM was faster than the simple kinetic model predicted which likely means that also precursors for the detected HOM, which were not observed by our instrument, were condensing. This further supported our hypothesis that a large fraction of HOM in the benzene system was produced via multiple OH oxidation steps.

Our study confirmed the formation of HOM from aromatic compounds both on short and long time scales. We have determined the HOM yield from benzene oxidation at relevant atmospheric lifetimes. In addition, we examined the phenol branching pathway and confirmed the production of nitrogen-containing HOM upon NO_X addition. Based on our findings, we conclude that HOM yield and composition is very sensitive to the reaction conditions. This sensitivity of HOM yield may partly explain the variability of SOA yield and time-dependency observed in previous studies. Based on current understanding of HOM as well as our SOA experiment result, we can suggest that HOM observed in this study may play an important role in initial particle growth in ambient atmosphere where aromatic VOC are abundant.

In addition, we ~~conclude that atmospheric models should take into account HOM yield dependence on the chemical regime when implementing quantitative laboratory results.~~ also conclude that more studies are required to fully understand how HOM yield and composition in aromatic systems depends on OH concentration and how the differences in HOM will affect the rate and magnitude of SOA formation. It would be valuable to sample different time scales, low and high reactant concentrations as well as effect of other important parameters, such as the effect of lights and NO_X. We also propose that future studies on aerosol formation from aromatic precursors would greatly benefit from including measurements of HOM in order to elucidate the detailed influence of experimental conditions on aromatic-derived highly oxygenated organic molecules and SOA, in the laboratory and the atmosphere.

Data availability. Data will be available from a persistent repository and upon request from corresponding authors

Appendix A: Modelled condensation of individual HOM

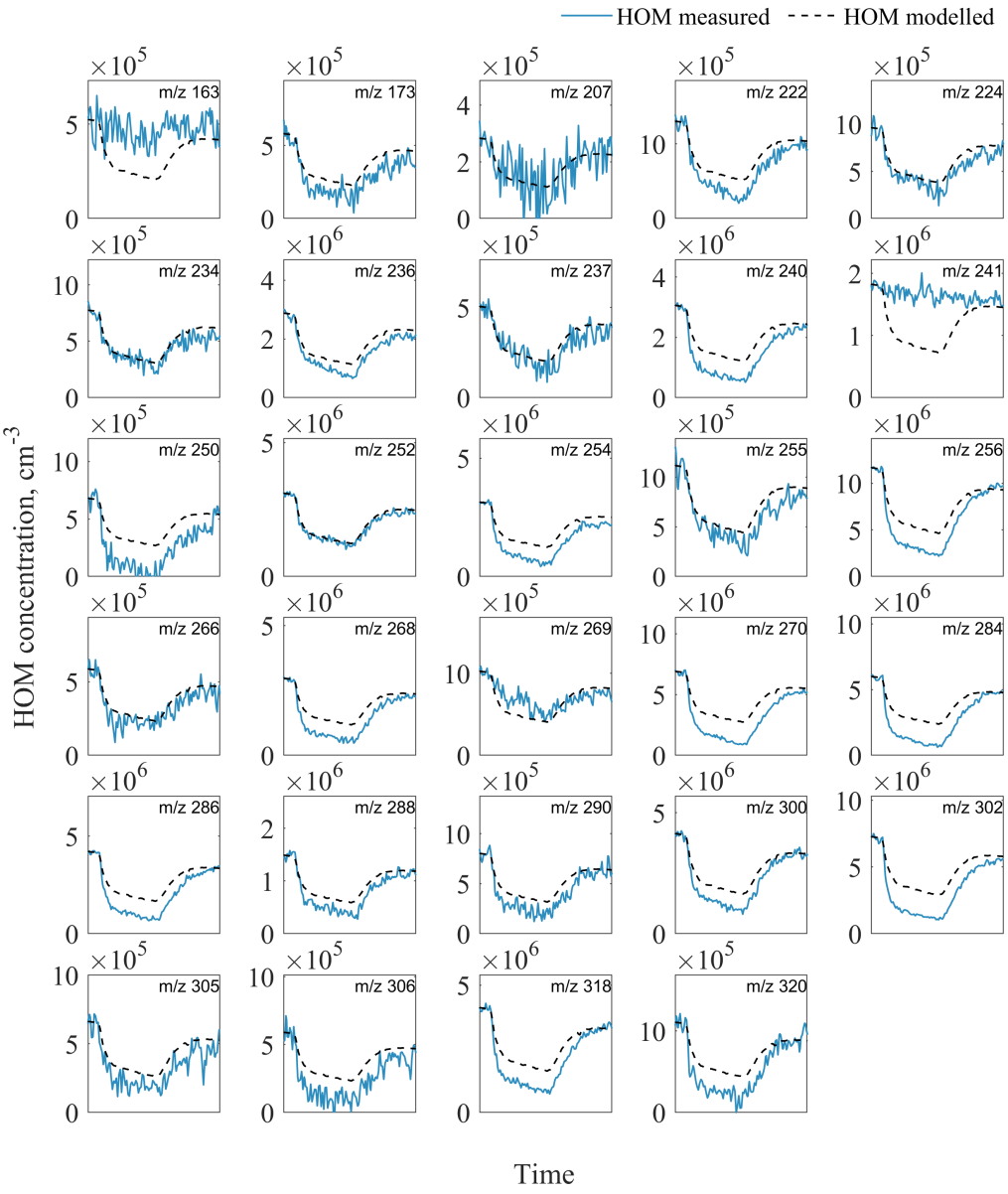

Figure A1. Evolution of measured and modelled HOM monomers during the seed addition experiment. The list of HOM compositions for each peak at corresponding m/z is presented in Table S4 in Supplement.

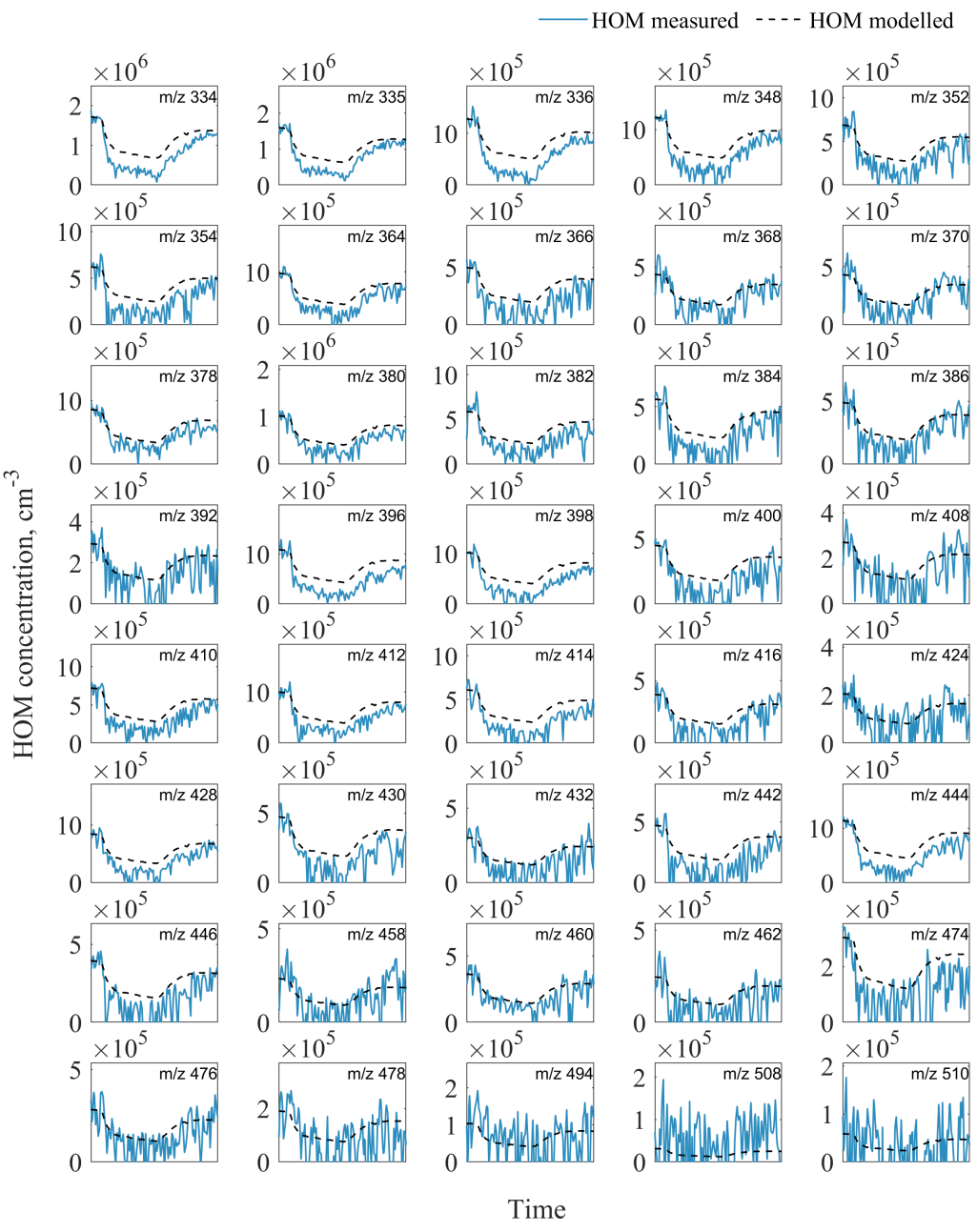

Figure A2. Evolution of measured and modelled HOM dimers during the seed addition experiment. The list of HOM compositions for each peak at corresponding m/z is presented in Table S4 in Supplement.

Author contributions. ME, MPR, TM, JW, EK, IP designed the experiments. Instrument deployment and operation were carried out by IP, SS, OK, RT, TJB, MP, ÅMH, EK, JW and TM; data analysis was done by OG, TM, SS and RT; OG interpreted the compiled data set. OG, ME and MPR wrote the paper. All co-authors discussed the results and commented the manuscript. The authors declare that they have no conflict of interest.

Competing interests. OK works for Kärsa Oy and SS works for TSI GmbH.

Acknowledgements. This study was supported by the European Research Council (grant 638703, "COALA") and the Academy of Finland (grants 299574, 317380 and 320094), and Academy of Finland Centre of Excellence program (project 272041 and 307331). OG acknowledges Doctoral School in Atmospheric Sciences at the University of Helsinki (ATM-DP) for financial support. ÅMH acknowledges Formas (grant number 214-2013-1430) and Vinnova, Sweden's Innovation Agency (grant number 2013-03058), including support for her research stay at Forschungszentrum Jülich. We also thank the tofTools team for providing tools for mass spectrometry data analysis.

References

Atkinson, R.: Kinetics and mechanisms of the gas-phase reactions of the hydroxyl radical with organic compounds, Journal of Physical and Chemical Reference Data, Monograph 1, 1–246, 1994a.

Atkinson, R.: Gas-Phase Tropospheric Chemistry of Organic Compounds, Journal of Physical and Chemical Reference Data, Monograph 2, 1–216, 1994b.

Atkinson, R.: Atmospheric chemistry of VOCs and NOx, Atmospheric Environment, 34, 2063–2101, https://doi.org/10.1016/s1352-2310(99)00460-4, 2000.

Atkinson, R. and Arey, J.: Atmospheric Degradation of Volatile Organic Compounds, Chemical Reviews, 103, 4605–4638, https://doi.org/10.1021/cr0206420, 2003.

Atkinson, R. and Aschmann, S. M.: Rate constants for the gas-phase reactions of the OH radical with a series of aromatic hydrocarbons at 296 ± 2 K, International Journal of Chemical Kinetics, 21, 355–365, https://doi.org/10.1002/kin.550210506, 1989.

Atkinson, R., Baulch, D. L., Cox, R. A., Crowley, J. N., Hampson, R. F., Hynes, R. G., Jenkin, M. E., Rossi, M. J., Troe, J., and Subcommittee, I.: Evaluated kinetic and photochemical data for atmospheric chemistry: Volume II –; gas phase reactions of organic species, Atmospheric Chemistry and Physics, 6, 3625–4055, https://doi.org/10.5194/acp-6-3625-2006, http://iupac.pole-ether.fr/, 2006.

Berndt, T. and Böge, O.: Formation of phenol and carbonyls from the atmospheric reaction of OH radicals with benzene, Physical Chemistry Chemical Physics, 8, 1205, https://doi.org/10.1039/b514148f, 2006.

Berndt, T., Richters, S., Kaethner, R., Voigtländer, J., Stratmann, F., Sipilä, M., Kulmala, M., and Herrmann, H.: Gas-Phase Ozonolysis of Cycloalkenes: Formation of Highly Oxidized RO2 Radicals and Their Reactions with NO, NO2, SO2, and Other RO2 Radicals, The Journal of Physical Chemistry A, 119, 10 336–10 348, https://doi.org/10.1021/acs.jpca.5b07295, 2015.

Berndt, T., Richters, S., Jokinen, T., Hyttinen, N., Kurtén, T., Otkjær, R. V., Kjaergaard, H. G., Stratmann, F., Herrmann, H., Sipilä, M., Kulmala, M., and Ehn, M.: Hydroxyl radical-induced formation of highly oxidized organic compounds, Nature Communications, 7, https://doi.org/10.1038/ncomms13677, 2016.

Berndt, T., Mentler, B., Scholz, W., Fischer, L., Herrmann, H., Kulmala, M., and Hansel, A.: Accretion Product Formation from Ozonolysis and OH Radical Reaction of α-Pinene: Mechanistic Insight and the Influence of Isoprene and Ethylene, Environmental Science & Technology, 52, 11 069–11 077, https://doi.org/10.1021/acs.est.8b02210, 2018a.

Berndt, T., Scholz, W., Mentler, B., Fischer, L., Herrmann, H., Kulmala, M., and Hansel, A.: Accretion Product Formation from Self- and Cross-Reactions of RO2 Radicals in the Atmosphere, Angewandte Chemie International Edition, 57, 3820–3824, https://doi.org/10.1002/anie.201710989, 2018b.

Bianchi, F., Kurtén, T., Riva, M., Mohr, C., Rissanen, M. P., Roldin, P., Berndt, T., Crounse, J. D., Wennberg, P. O., Mentel, T. F., Wildt, J., Junninen, H., Jokinen, T., Kulmala, M., Worsnop, D. R., Thornton, J. A., Donahue, N., Kjaergaard, H. G., and Ehn, M.: Highly Oxygenated Organic Molecules (HOM) from Gas-Phase Autoxidation Involving Peroxy Radicals: A Key Contributor to Atmospheric Aerosol, Chemical Reviews, 119, 3472–3509, https://doi.org/10.1021/acs.chemrev.8b00395, 2019.

Birdsall, A. W. and Elrod, M. J.: Comprehensive NO-Dependent Study of the Products of the Oxidation of Atmospherically Relevant Aromatic Compounds, The Journal of Physical Chemistry A, 115, 5397–5407, https://doi.org/10.1021/jp2010327, 2011.

Birdsall, A. W., Andreoni, J. F., and Elrod, M. J.: Investigation of the Role of Bicyclic Peroxy Radicals in the Oxidation Mechanism of Toluene, The Journal of Physical Chemistry A, 114, 10 655–10 663, https://doi.org/10.1021/jp105467e, 2010.

Bloss, C., Wagner, V., Jenkin, M. E., Volkamer, R., Bloss, W. J., Lee, J. D., Heard, D. E., Wirtz, K., Martin-Reviejo, M., Rea, G., Wenger, J. C., and Pilling, M. J.: Development of a detailed chemical mechanism (MCMv3.1) for the atmospheric oxidation of aromatic hydrocarbons, Atmospheric Chemistry and Physics, 5, 641–664, https://doi.org/10.5194/acp-5-641-2005, 2005.

Calvert, J. G., Atkinson, R., Becker, K. H., Kamens, R. M., Seinfeld, J. H., Wallington, T. J., and Yarwood, G.: The Mechanisms of Atmospheric Oxidation of the Aromatic Hydrocarbons, Oxford University Press, 2002.

Chacon-Madrid, H. J. and Donahue, N. M.: Fragmentation vs. functionalization: chemical aging and organic aerosol formation, Atmospheric Chemistry and Physics, 11, 10 553–10 563, https://doi.org/10.5194/acp-11-10553-2011, 2011.

Crounse, J. D., Knap, H. C., Ørnsø, K. B., Jørgensen, S., Paulot, F., Kjaergaard, H. G., and Wennberg, P. O.: Atmospheric Fate of Methacrolein. 1. Peroxy Radical Isomerization Following Addition of OH and O2, The Journal of Physical Chemistry A, 116, 5756–5762, https://doi.org/10.1021/jp211560u, 2012.

Crounse, J. D., Nielsen, L. B., Jørgensen, S., Kjaergaard, H. G., and Wennberg, P. O.: Autoxidation of Organic Compounds in the Atmosphere, The Journal of Physical Chemistry Letters, 4, 3513–3520, https://doi.org/10.1021/jz4019207, 2013.

DeCarlo, P. F., Kimmel, J. R., Trimborn, A., Northway, M. J., Jayne, J. T., Aiken, A. C., Gonin, M., Fuhrer, K., Horvath, T., Docherty, K. S., Worsnop, D. R., and Jimenez, J. L.: Field-Deployable, High-Resolution, Time-of-Flight Aerosol Mass Spectrometer, Analytical Chemistry, 78, 8281–8289, https://doi.org/10.1021/ac061249n, 2006.

Ehn, M., Thornton, J. A., Kleist, E., Sipilä, M., Junninen, H., Pullinen, I., Springer, M., Rubach, F., Tillmann, R., Lee, B., Lopez-Hilfiker, F., Andres, S., Acir, I.-H., Rissanen, M., Jokinen, T., Schobesberger, S., Kangasluoma, J., Kontkanen, J., Nieminen, T., Kurtén, T., Nielsen, L. B., Jørgensen, S., Kjaergaard, H. G., Canagaratna, M., Maso, M. D., Berndt, T., Petäjä, T., Wahner, A., Kerminen, V.-M., Kulmala, M., Worsnop, D. R., Wildt, J., and Mentel, T. F.: A large source of low-volatility secondary organic aerosol, Nature, 506, 476–479, https://doi.org/10.1038/nature13032, 2014.

Emanuelsson, E. U., Hallquist, M., Kristensen, K., Glasius, M., Bohn, B., Fuchs, H., Kammer, B., Kiendler-Scharr, A., Nehr, S., Rubach, F., Tillmann, R., Wahner, A., Wu, H.-C., and Mentel, T. F.: Formation of anthropogenic secondary organic aerosol (SOA) and its influence on biogenic SOA properties, Atmospheric Chemistry and Physics, 13, 2837–2855, https://doi.org/10.5194/acp-13-2837-2013, 2013.

Finlayson-Pitts, B. J. and Pitts, J. N. J.: Chemistry of the Upper and Lower Atmosphere: Theory, Experiments, and Applications, Academic Press, 2000.

Fuller, E. N., Schettler, P. D., and Giddings, J. C.: New method for prediction of binary gas-phase diffusion coefficients, Industrial & Engineering Chemistry, 58, 18–27, https://doi.org/10.1021/ie50677a007, 1966.

Gautrois, M. and Koppmann, R.: Diffusion technique for the production of gas standards for atmospheric measurements, Journal of Chromatography A, 848, 239–249, https://doi.org/10.1016/s0021-9673(99)00424-0, 1999.

Glowacki, D. R. and Pilling, M. J.: Unimolecular Reactions of Peroxy Radicals in Atmospheric Chemistry and Combustion, ChemPhysChem, 11, 3836–3843, https://doi.org/10.1002/cphc.201000469, 2010.

Glowacki, D. R., Wang, L., and Pilling, M. J.: Evidence of Formation of Bicyclic Species in the Early Stages of Atmospheric Benzene Oxidation, The Journal of Physical Chemistry A, 113, 5385–5396, https://doi.org/10.1021/jp9001466, 2009.

Graus, M., Müller, M., and Hansel, A.: High resolution PTR-TOF: Quantification and formula confirmation of VOC in real time, Journal of the American Society for Mass Spectrometry, 21, 1037–1044, https://doi.org/10.1016/j.jasms.2010.02.006, 2010.

Hildebrandt, L., Donahue, N. M., and Pandis, S. N.: High formation of secondary organic aerosol from the photo-oxidation of toluene, Atmospheric Chemistry and Physics, 9, 2973–2986, https://doi.org/10.5194/acp-9-2973-2009, 2009.

Hyttinen, N., Kupiainen-Määttä, O., Rissanen, M. P., Muuronen, M., Ehn, M., and Kurtén, T.: Modeling the Charging of Highly Oxidized Cyclohexene Ozonolysis Products Using Nitrate-Based Chemical Ionization, The Journal of Physical Chemistry A, 119, 6339–6345, https://doi.org/10.1021/acs.jpca.5b01818, 2015.

Hyttinen, N., Otkjær, R. V., Iyer, S., Kjaergaard, H. G., Rissanen, M. P., Wennberg, P. O., and Kurtén, T.: Computational Comparison of Different Reagent Ions in the Chemical Ionization of Oxidized Multifunctional Compounds, The Journal of Physical Chemistry A, 122, 269–279, https://doi.org/10.1021/acs.jpca.7b10015, 2017.

Jenkin, M. E., Saunders, S. M., Wagner, V., and Pilling, M. J.: Protocol for the development of the Master Chemical Mechanism, MCM v3 (Part B): tropospheric degradation of aromatic volatile organic compounds, Atmospheric Chemistry and Physics, 3, 181–193, https://doi.org/10.5194/acp-3-181-2003, 2003.

Jokinen, T., Sipilä, M., Junninen, H., Ehn, M., Lönn, G., Hakala, J., Petäjä, T., Mauldin, R. L., Kulmala, M., and Worsnop, D. R.: Atmospheric sulphuric acid and neutral cluster measurements using CI-APi-TOF, Atmospheric Chemistry and Physics, 12, 4117–4125, https://doi.org/10.5194/acp-12-4117-2012, 2012.

Jokinen, T., Sipilä, M., Richters, S., Kerminen, V.-M., Paasonen, P., Stratmann, F., Worsnop, D., Kulmala, M., Ehn, M., Herrmann, H., and Berndt, T.: Rapid Autoxidation Forms Highly Oxidized RO2Radicals in the Atmosphere, Angewandte Chemie International Edition, 53, 14 596–14 600, https://doi.org/10.1002/anie.201408566, 2014.

Jokinen, T., Berndt, T., Makkonen, R., Kerminen, V.-M., Junninen, H., Paasonen, P., Stratmann, F., Herrmann, H., Guenther, A. B., Worsnop, D. R., Kulmala, M., Ehn, M., and Sipilä, M.: Production of extremely low volatile organic compounds from biogenic emissions: Measured yields and atmospheric implications, Proceedings of the National Academy of Sciences, 112, 7123–7128, https://doi.org/10.1073/pnas.1423977112, 2015.

Junninen, H.: Data cycle in atmospheric physics : From detected millivolts to understanding the atmosphere, Thesis, http://urn.fi/URN:ISBN:978-952-5822-81-6, 2013.

Junninen, H., Ehn, M., Petäjä, T., Luosujärvi, L., Kotiaho, T., Kostiainen, R., Rohner, U., Gonin, M., Fuhrer, K., Kulmala, M., and Worsnop, D. R.: A high-resolution mass spectrometer to measure atmospheric ion composition, Atmospheric Measurement Techniques, 3, 1039–1053, https://doi.org/10.5194/amt-3-1039-2010, 2010.

Kokkola, H., Yli-Pirilä, P., Vesterinen, M., Korhonen, H., Keskinen, H., Romakkaniemi, S., Hao, L., Kortelainen, A., Joutsensaari, J., Worsnop, D. R., Virtanen, A., and Lehtinen, K. E. J.: The role of low volatile organics on secondary organic aerosol formation, Atmospheric Chemistry and Physics, 14, 1689–1700, https://doi.org/10.5194/acp-14-1689-2014, 2014.

Kroll, J. H. and Seinfeld, J. H.: Chemistry of secondary organic aerosol: Formation and evolution of low-volatility organics in the atmosphere, Atmospheric Environment, 42, 3593–3624, https://doi.org/10.1016/j.atmosenv.2008.01.003, 2008.

Kulmala, M., Petäjä, T., Nieminen, T., Sipilä, M., Manninen, H. E., Lehtipalo, K., Maso, M. D., Aalto, P. P., Junninen, H., Paasonen, P., Riipinen, I., Lehtinen, K. E. J., Laaksonen, A., and Kerminen, V.-M.: Measurement of the nucleation of atmospheric aerosol particles, Nature Protocols, 7, 1651–1667, https://doi.org/10.1038/nprot.2012.091, 2012.

Lay, T. H., Bozzelli, J. W., and Seinfeld, J. H.: Atmospheric Photochemical Oxidation of Benzene: Benzene + OH and the Benzene-OH Adduct (Hydroxyl-2, 4-cyclohexadienyl) + O2, The Journal of Physical Chemistry, 100, 6543–6554, https://doi.org/10.1021/jp951726y, 1996.

Lehtipalo, K., Yan, C., Dada, L., Bianchi, F., Xiao, M., Wagner, R., Stolzenburg, D., Ahonen, L. R., Amorim, A., Baccarini, A., Bauer, P. S., Baumgartner, B., Bergen, A., Bernhammer, A.-K., Breitenlechner, M., Brilke, S., Buchholz, A., Mazon, S. B., Chen, D., Chen, X., Dias, A., Dommen, J., Draper, D. C., Duplissy, J., Ehn, M., Finkenzeller, H., Fischer, L., Frege, C., Fuchs, C., Garmash, O., Gordon, H., Hakala,

J., He, X., Heikkinen, L., Heinritzi, M., Helm, J. C., Hofbauer, V., Hoyle, C. R., Jokinen, T., Kangasluoma, J., Kerminen, V.-M., Kim, C., Kirkby, J., Kontkanen, J., Kürten, A., Lawler, M. J., Mai, H., Mathot, S., Mauldin, R. L., Molteni, U., Nichman, L., Nie, W., Nieminen, T., Ojdanic, A., Onnela, A., Passananti, M., Petäjä, T., Piel, F., Pospisilova, V., Quéléver, L. L. J., Rissanen, M. P., Rose, C., Sarnela, N., Schallhart, S., Schuchmann, S., Sengupta, K., Simon, M., Sipilä, M., Tauber, C., Tomé, A., Tröstl, J., Väisänen, O., Vogel, A. L., Volkamer, R., Wagner, A. C., Wang, M., Weitz, L., Wimmer, D., Ye, P., Ylisirniö, A., Zha, Q., Carslaw, K. S., Curtius, J., Donahue, N. M., Flagan, R. C., Hansel, A., Riipinen, I., Virtanen, A., Winkler, P. M., Baltensperger, U., Kulmala, M., and Worsnop, D. R.: Multicomponent new particle formation from sulfuric acid, ammonia, and biogenic vapors, Science Advances, 4, eaau5363, https://doi.org/10.1126/sciadv.aau5363, 2018.

Lindinger, W., Hansel, A., and Jordan, A.: On-line monitoring of volatile organic compounds at pptv levels by means of proton-transfer-reaction mass spectrometry (PTR-MS) medical applications, food control and environmental research, International Journal of Mass Spectrometry and Ion Processes, 173, 191–241, https://doi.org/10.1016/s0168-1176(97)00281-4, 1998.

Liu, P.-W. G., Yao, Y.-C., Tsai, J.-H., Hsu, Y.-C., Chang, L.-P., and Chang, K.-H.: Source impacts by volatile organic compounds in an industrial city of southern Taiwan, Science of The Total Environment, 398, 154–163, https://doi.org/10.1016/j.scitotenv.2008.02.053, 2008.

McFiggans, G., Mentel, T. F., Wildt, J., Pullinen, I., Kang, S., Kleist, E., Schmitt, S., Springer, M., Tillmann, R., Wu, C., Zhao, D., Hallquist, M., Faxon, C., Le Breton, M., Hallquist, s. M., Simpson, D., Bergström, R., Jenkin, M. E., Ehn, M., Thornton, J. A., Alfarra, M. R., Bannan, T. J., Percival, C. J., Priestley, M., Topping, D., and Kiendler-Scharr, A.: Secondary organic aerosol reduced by mixture of atmospheric vapours, Nature, 565, 587–593, https://doi.org/10.1038/s41586-018-0871-y, https://doi.org/10.1038/s41586-018-0871-y, 2019.

Mentel, T. F., Wildt, J., Kiendler-Scharr, A., Kleist, E., Tillmann, R., Maso, M. D., Fisseha, R., Hohaus, T., Spahn, H., Uerlings, R., Wegener, R., Griffiths, P. T., Dinar, E., Rudich, Y., and Wahner, A.: Photochemical production of aerosols from real plant emissions, Atmospheric Chemistry and Physics, 9, 4387–4406, https://doi.org/10.5194/acp-9-4387-2009, 2009.

Mentel, T. F., Springer, M., Ehn, M., Kleist, E., Pullinen, I., Kurtén, T., Rissanen, M., Wahner, A., and Wildt, J.: Formation of highly oxidized multifunctional compounds: autoxidation of peroxy radicals formed in the ozonolysis of alkenes – deduced from structure–product relationships, Atmospheric Chemistry and Physics, 15, 6745–6765, https://doi.org/10.5194/acp-15-6745-2015, 2015.

Misztal, P., Hewitt, C., Wildt, J., Blande, J., Eller, A., Fares, S., Gentner, D., Gilman, J., Graus, M., Greenberg, J., Guenther, A., Hansel, A., Harley, P., Huang, M., Jardine, K., Karl, T., Kaser, L., Keutsch, F., Kiendler-Scharr, A., Kleist, E., Lerner, B., Li, T., Mak, J., Nölscher, A., Schnitzhofer, R., Sinha, V., Thornton, B., Warneke, C., Wegener, F., Werner, C., Williams, J., Worton, D., Yassaa, N., and Goldstein, A.: Atmospheric benzenoid emissions from plants rival those from fossil fuels, Scientific Reports, 5, https://doi.org/10.1038/srep12064, 2015.

Molteni, U., Bianchi, F., Klein, F., Haddad, I. E., Frege, C., Rossi, M. J., Dommen, J., and Baltensperger, U.: Formation of highly oxygenated organic molecules from aromatic compounds, Atmospheric Chemistry and Physics, 18, 1909–1921, https://doi.org/10.5194/acp-18-1909-2018, 2018.

Ng, N. L., Kroll, J. H., Chan, A. W. H., Chhabra, P. S., Flagan, R. C., and Seinfeld, J. H.: Secondary organic aerosol formation from m-xylene, toluene, and benzene, Atmospheric Chemistry and Physics, 7, 3909–3922, https://doi.org/10.5194/acp-7-3909-2007, 2007.

Olariu, R. I., Klotz, B., Barnes, I., Becker, K. H., and Mocanu, R.: FT–IR study of the ring-retaining products from the reaction of OH radicals with phenol, o-, m-, and p-cresol, Atmospheric Environment, 36, 3685–3697, https://doi.org/10.1016/s1352-2310(02)00202-9, 2002.

Orlando, J. J. and Tyndall, G. S.: Laboratory studies of organic peroxy radical chemistry: an overview with emphasis on recent issues of atmospheric significance, Chemical Society Reviews, 41, 6294, https://doi.org/10.1039/c2cs35166h, 2012.

Orlando, J. J., Tyndall, G. S., and Wallington, T. J.: The Atmospheric Chemistry of Alkoxy Radicals, Chemical Reviews, 103, 4657–4690, https://doi.org/10.1021/cr020527p, 2003.

Öström, E., Putian, Z., Schurgers, G., Mishurov, M., Kivekäs, N., Lihavainen, H., Ehn, M., Rissanen, M. P., Kurtén, T., Boy, M., Swietlicki, E., and Roldin, P.: Modeling the role of highly oxidized multifunctional organic molecules for the growth of new particles over the boreal forest region, Atmospheric Chemistry and Physics, 17, 8887–8901, https://doi.org/10.5194/acp-17-8887-2017, 2017.

Praske, E., Otkjær, R. V., Crounse, J. D., Hethcox, J. C., Stoltz, B. M., Kjaergaard, H. G., and Wennberg, P. O.: Atmospheric autoxidation is increasingly important in urban and suburban North America, Proceedings of the National Academy of Sciences, 115, 64–69, https://doi.org/10.1073/pnas.1715540115, 2018.

Rissanen, M. P.: NO2 Suppression of Autoxidation–Inhibition of Gas-Phase Highly Oxidized Dimer Product Formation, ACS Earth and Space Chemistry, 2, 1211–1219, https://doi.org/10.1021/acsearthspacechem.8b00123, 2018.

Rissanen, M. P., Kurtén, T., Sipilä, M., Thornton, J. A., Kangasluoma, J., Sarnela, N., Junninen, H., Jørgensen, S., Schallhart, S., Kajos, M. K., Taipale, R., Springer, M., Mentel, T. F., Ruuskanen, T., Petäjä, T., Worsnop, D. R., Kjaergaard, H. G., and Ehn, M.: The Formation of Highly Oxidized Multifunctional Products in the Ozonolysis of Cyclohexene, Journal of the American Chemical Society, 136, 15 596–15 606, https://doi.org/10.1021/ja507146s, 2014.

Rissanen, M. P., Kurtén, T., Sipilä, M., Thornton, J. A., Kausiala, O., Garmash, O., Kjaergaard, H. G., Petäjä, T., Worsnop, D. R., Ehn, M., and Kulmala, M.: Effects of Chemical Complexity on the Autoxidation Mechanisms of Endocyclic Alkene Ozonolysis Products: From Methylcyclohexenes toward Understanding α-Pinene, The Journal of Physical Chemistry A, 119, 4633–4650, https://doi.org/10.1021/jp510966g, 2015.

Rubach, F.: Aerosol processes in the Planetary Boundary Layer: High resolution Aerosol Mass Spectrometry on a Zeppelin NT Airship, Dr., Wuppertal, Jülich, http://hdl.handle.net/2128/5160, wuppertal, Diss., 2013, 2013.

Schwantes, R. H., Schilling, K. A., McVay, R. C., Lignell, H., Coggon, M. M., Zhang, X., Wennberg, P. O., and Seinfeld, J. H.: Formation of highly oxygenated low-volatility products from cresol oxidation, Atmospheric Chemistry and Physics, 17, 3453–3474, https://doi.org/10.5194/acp-17-3453-2017, 2017.

Tröstl, J., Chuang, W. K., Gordon, H., Heinritzi, M., Yan, C., Molteni, U., Ahlm, L., Frege, C., Bianchi, F., Wagner, R., Simon, M., Lehtipalo, K., Williamson, C., Craven, J. S., Duplissy, J., Adamov, A., Almeida, J., Bernhammer, A.-K., Breitenlechner, M., Brilke, S., Dias, A., Ehrhart, S., Flagan, R. C., Franchin, A., Fuchs, C., Guida, R., Gysel, M., Hansel, A., Hoyle, C. R., Jokinen, T., Junninen, H., Kangasluoma, J., Keskinen, H., Kim, J., Krapf, M., Kürten, A., Laaksonen, A., Lawler, M., Leiminger, M., Mathot, S., Möhler, O., Nieminen, T., Onnela, A., Petäjä, T., Piel, F. M., Miettinen, P., Rissanen, M. P., Rondo, L., Sarnela, N., Schobesberger, S., Sengupta, K., Sipilä, M., Smith, J. N., Steiner, G., Tomè, A., Virtanen, A., Wagner, A. C., Weingartner, E., Wimmer, D., Winkler, P. M., Ye, P., Carslaw, K. S., Curtius, J., Dommen, J., Kirkby, J., Kulmala, M., Riipinen, I., Worsnop, D. R., Donahue, N. M., and Baltensperger, U.: The role of low-volatility organic compounds in initial particle growth in the atmosphere, Nature, 533, 527–531, https://doi.org/10.1038/nature18271, 2016.

Vereecken, L.: Reaction Mechanisms for the Atmospheric Oxidation of Monocyclic Aromatic Compounds, in: Advances in Atmospheric Chemistry, pp. 377–527, WORLD SCIENTIFIC, https://doi.org/10.1142/9789813271838_0006, 2019.

Vereecken, L. and Peeters, J.: Decomposition of substituted alkoxy radicals—part I: a generalized structure–activity relationship for reaction barrier heights, Physical Chemistry Chemical Physics, 11, 9062, https://doi.org/10.1039/b909712k, 2009.

Volkamer, R., Klotz, B., Barnes, I., Imamura, T., Wirtz, K., Washida, N., Becker, K. H., and Platt, U.: OH-initiated oxidation of benzene, Physical Chemistry Chemical Physics, 4, 1598–1610, https://doi.org/10.1039/b108747a, 2002.

Wang, L., Wu, R., and Xu, C.: Atmospheric Oxidation Mechanism of Benzene. Fates of Alkoxy Radical Intermediates and Revised Mechanism, The Journal of Physical Chemistry A, 117, 14 163–14 168, https://doi.org/10.1021/jp4101762, 2013.

Wang, S., Wu, R., Berndt, T., Ehn, M., and Wang, L.: Formation of Highly Oxidized Radicals and Multifunctional Products from the Atmospheric Oxidation of Alkylbenzenes, Environmental Science & Technology, 51, 8442–8449, https://doi.org/10.1021/acs.est.7b02374, 2017.

Yan, C., Nie, W., Äijälä, M., Rissanen, M. P., Canagaratna, M. R., Massoli, P., Junninen, H., Jokinen, T., Sarnela, N., Häme, S. A. K., Schobesberger, S., Canonaco, F., Yao, L., Prévôt, A. S. H., Petäjä, T., Kulmala, M., Sipilä, M., Worsnop, D. R., and Ehn, M.: Source characterization of highly oxidized multifunctional compounds in a boreal forest environment using positive matrix factorization, Atmospheric Chemistry and Physics, 16, 12 715–12 731, https://doi.org/10.5194/acp-16-12715-2016, 2016.

Zabel, F.: Unimolecular Decomposition of Peroxynitrates, Zeitschrift für Physikalische Chemie, 188, 119–142, https://doi.org/10.1524/zpch.1995.188.part_1_2.119, 1995.

Zhang, X., Cappa, C. D., Jathar, S. H., McVay, R. C., Ensberg, J. J., Kleeman, M. J., and Seinfeld, J. H.: Influence of vapor wall loss in laboratory chambers on yields of secondary organic aerosol, Proceedings of the National Academy of Sciences, 111, 5802–5807, https://doi.org/10.1073/pnas.1404727111, 2014.

Tables in Supplement present the spectra shown in Fig. 3 and 5 and lists the molecular composition as well as exact mass of the individual oxidation products as identified in CI-APi-TOF spectra. If two compounds overlapped on the same integer mass, the value was assigned to the dominant peak, while the value for the other one was set to "n/a".

Table S1. Products of benzene oxidation as identified in CI-APi-TOF spectra from the flow reactor. Data corresponds to Fig. 3a in the main text. All ions are negatively charged and include the reagent ion, NO_3^-. m/z is mass-to-charge ratio and f_{total} is fraction of total signal.

C	H	O	N	m/z, Th	$f_{total}x10^{-4}$	C	H	O	N	m/z, Th	$f_{total}x10^{-4}$
6	6	7	1	204.0150	9.4	6	6	13	1	299.9845	8.9
6	7	7	1	205.0228	3.1	6	7	13	1	300.9923	2.7
6	8	7	1	206.0306	22.5	6	8	13	1	302.0001	15.6
5	6	8	1	208.0099	3.1	12	12	9	1	314.0518	3.2
6	6	8	1	220.0099	6.3	6	6	14	1	315.9794	n/a
6	7	8	1	221.0177	0.8	12	14	9	1	316.0674	2.5
6	8	8	1	222.0255	55.9	6	7	14	1	316.9872	47.8
5	5	9	1	222.9970	5.5	6	8	14	1	317.9950	28.5
5	6	9	1	224.0048	9.2	12	12	10	1	330.0467	1.1
5	7	9	1	225.0126	1.6	6	6	15	1	331.9743	3.2
6	6	9	1	236.0048	5.4	12	14	10	1	332.0623	n/a
6	7	9	1	237.0126	1.2	6	7	15	1	332.9821	0.8
6	8	9	1	238.0205	10.2	6	8	15	1	333.9899	2.9
5	6	10	1	239.9997	38.3	12	14	11	1	348.0572	89.1
5	7	10	1	241.0075	4.9	6	8	16	1	349.9849	5.6
5	8	10	1	242.0154	7.9	11	14	12	1	352.0522	6.9
6	6	10	1	251.9997	1.4	10	12	13	1	354.0314	4.6
6	7	10	1	253.0075	2.6	12	12	12	1	362.0365	1.0
6	8	10	1	254.0154	17.8	12	14	12	1	364.0522	5.5
5	6	11	1	255.9946	91.1	11	14	13	1	368.0471	4.0
5	7	11	1	257.0025	7.5	12	12	13	1	378.0314	4.6
6	6	11	1	267.9946	4.7	12	14	13	1	380.0471	24.6
6	7	11	1	269.0025	0.7	11	14	14	1	384.0420	2.5
6	8	11	1	270.0103	68.4	12	14	14	1	396.0420	2.0
5	6	12	1	271.9896	7.4	11	12	15	1	398.0212	0.8
5	7	12	1	272.9974	3.4	11	14	15	1	400.0369	0.9
5	8	12	1	274.0052	2.8	12	12	15	1	410.0212	0.7
6	6	12	1	283.9896	2.9	12	14	15	1	412.0369	65.4
6	7	12	1	284.9974	51.4	11	14	16	1	416.0318	2.3
6	8	12	1	286.0052	87.5	12	14	16	1	428.0318	2.0
5	8	13	1	290.0001	3.2	12	14	17	1	444.0267	16.5

Table S2. Products of toluene oxidation as identified in CI-APi-TOF spectra from the flow reactor. Data corresponds to Fig. 3b in the main text. All ions are negatively charged and include the reagent ion, NO_3^-. m/z is mass-to-charge ratio and f_{total} is fraction of total signal.

C	H	O	N	m/z, Th	$f_{total}x10^{-4}$	C	H	O	N	m/z, Th	$f_{total}x10^{-4}$
7	8	5	1	186.0408	5.1	11	14	10	1	320.0623	9.3
7	8	6	1	202.0357	212.2	13	14	9	1	328.0674	45.2
6	6	7	1	204.0150	25.2	13	16	9	1	330.0831	10.1
7	10	6	1	204.0514	n/a	12	14	10	1	332.0623	73.0
6	8	7	1	206.0306	19.2	12	16	10	1	334.0780	3.2
5	8	8	1	210.0255	5.7	11	14	11	1	336.0572	4.4
7	8	7	1	218.0306	80.4	14	16	9	1	342.0831	49.7
7	9	7	1	219.0385	18.8	14	18	9	1	344.0987	29.5
6	6	8	1	220.0099	n/a	14	20	9	1	346.1144	77.9
7	10	7	1	220.0463	139.3	12	14	11	1	348.0572	39.9
6	8	8	1	222.0255	14.8	11	14	12	1	352.0522	3.5
7	12	7	1	222.0619	n/a	14	14	10	1	356.0623	19.6
5	6	9	1	224.0048	10.9	14	16	10	1	358.0780	45.8
6	10	8	1	224.0412	n/a	14	18	10	1	360.0936	29.4
7	8	8	1	234.0255	171.5	13	16	11	1	362.0729	11.5
6	6	9	1	236.0048	n/a	13	18	11	1	364.0885	13.9
7	10	8	1	236.0412	741.2	11	14	13	1	368.0471	15.0
6	8	9	1	238.0205	42.6	14	16	11	1	374.0729	276.7
7	12	8	1	238.0568	n/a	14	18	11	1	376.0885	349.0
5	6	10	1	239.9997	n/a	13	16	12	1	378.0678	36.7
6	10	9	1	240.0361	17.7	13	18	12	1	380.0834	12.8
5	7	10	1	241.0075	10.5	14	14	12	1	388.0522	6.2
7	8	9	1	250.0205	52.2	14	16	12	1	390.0678	66.5
6	6	10	1	251.9997	n/a	14	18	12	1	392.0834	80.2
7	10	9	1	252.0361	161.1	13	16	13	1	394.0627	12.9
6	8	10	1	254.0154	43.4	14	20	12	1	394.0991	n/a
7	12	9	1	254.0518	n/a	13	18	13	1	396.0784	7.7
5	6	11	1	255.9946	n/a	14	14	13	1	404.0471	0.8
6	10	10	1	256.0310	19.1	14	16	13	1	406.0627	61.6
7	8	10	1	266.0154	66.5	14	18	13	1	408.0784	42.7
6	6	11	1	267.9946	n/a	14	20	13	1	410.0940	17.8
7	10	10	1	268.0310	129.9	14	16	14	1	422.0576	21.6
6	8	11	1	270.0103	41.8	14	18	14	1	424.0733	29.5
7	12	10	1	270.0467	n/a	14	20	14	1	426.0889	1.4
7	8	11	1	282.0103	52.9	14	16	15	1	438.0526	8.2
6	6	12	1	283.9896	n/a	14	18	15	1	440.0682	62.0
7	10	11	1	284.0259	140.4	14	20	15	1	442.0838	4.6
6	8	12	1	286.0052	24.1	14	16	16	1	454.0475	5.4
7	12	11	1	286.0416	n/a	14	18	16	1	456.0631	4.4
7	8	12	1	298.0052	26.2	14	16	17	1	470.0424	3.1
7	9	12	1	299.0130	35.6	14	18	17	1	472.0580	3.1
7	10	12	1	300.0208	87.5	14	16	18	1	486.0373	0.9
7	8	13	1	314.0001	26.6						

Table S3. Products of naphthalene oxidation as identified in CI-APi-TOF spectra from the flow reactor. Data corresponds to Fig. 3c in the main text. All ions are negatively charged and include the reagent ion, NO_3^-. m/z is mass-to-charge ratio and f_{total} is fraction of total signal.

C	H	O	N	m/z, Th	$f_{total}x10^{-4}$	C	H	O	N	m/z, Th	$f_{total}x10^{-4}$
10	10	7	1	256.0463	80.7	20	18	8	1	400.1038	14.9
10	8	8	1	270.0255	4.7	20	16	9	1	414.0831	3.7
10	10	8	1	272.0412	39.5	20	18	9	1	416.0987	70.7
10	12	8	1	274.0569	22.3	20	20	9	1	418.1144	41.1
10	8	9	1	286.0205	6.3	20	16	10	1	430.0780	5.6
10	10	9	1	288.0361	64.9	20	18	10	1	432.0936	23.2
10	11	9	1	289.0439	26.4	20	20	10	1	434.1093	133.5
10	12	9	1	290.0518	182.8	20	16	11	1	446.0729	4.0
10	8	10	1	302.0154	4.1	20	17	11	1	447.0807	4.1
10	9	10	1	303.0232	0.9	20	18	11	1	448.0885	23.2
10	10	10	1	304.0310	46.2	20	20	11	1	450.1042	93.7
10	11	10	1	305.0389	10.9	20	21	11	1	451.1120	85.4
10	12	10	1	306.0467	143.1	20	22	11	1	452.1198	28.3
10	14	10	1	308.0623	18.8	20	16	12	1	462.0678	3.7
10	8	11	1	318.0103	3.1	20	18	12	1	464.0834	14.8
10	9	11	1	319.0181	1.6	20	20	12	1	466.0991	76.2
10	10	11	1	320.0259	28.7	20	22	12	1	468.1148	31.5
10	12	11	1	322.0416	93.5	20	16	13	1	478.0627	1.5
10	14	11	1	324.0572	47.5	20	18	13	1	480.0784	10.6
10	15	11	1	325.0651	17.0	20	20	13	1	482.0940	47.5
10	8	12	1	334.0052	3.2	20	21	13	1	483.1018	30.6
10	9	12	1	335.0130	2.5	20	22	13	1	484.1097	39.9
10	10	12	1	336.0208	16.2	20	23	13	1	485.1175	21.8
10	11	12	1	337.0287	7.1	20	24	13	1	486.1253	8.1
10	12	12	1	338.0365	50.7	20	16	14	1	494.0576	0.6
10	13	12	1	339.0443	21.0	20	18	14	1	496.0733	7.4
10	14	12	1	340.0522	42.0	20	20	14	1	498.0889	20.9
10	15	12	1	341.0600	10.7	20	21	14	1	499.0967	10.3
10	10	13	1	352.0158	11.9	20	22	14	1	500.1046	28.0
10	12	13	1	354.0314	24.4	20	23	14	1	501.1124	36.5
10	13	13	1	355.0393	7.1	20	24	14	1	502.1202	11.5
10	14	13	1	356.0471	20.8	20	18	15	1	512.0682	4.6
10	15	13	1	357.0549	8.2	20	20	15	1	514.0839	16.1
10	10	14	1	368.0107	5.7	20	22	15	1	516.0995	17.1
20	18	6	1	368.1140	n/a	20	23	15	1	517.1073	15.8
10	12	14	1	370.0263	13.0	20	24	15	1	518.1151	12.8
10	13	14	1	371.0342	4.0	20	20	16	1	530.0787	7.1
10	14	14	1	372.0420	9.4	20	22	16	1	532.0944	9.4
10	15	14	1	373.0498	4.0	20	20	17	1	546.0737	4.6
20	18	7	1	384.1089	102.1	20	22	17	1	548.0893	4.7

Table S4. Peaks identified in JPAC. Non-nitrogen containing HOM were included in HOM yield calculation and kinetic model for seeded experiment, with exception of those marked with * in m/z column. All ions are negatively charged and include the reagent ion. In non-nitrogen containing HOM, N content of 1 indicates that the HOM is likely charged by NO_3^-, while if N=0, the HOM are detected as de-protonated species. Among nitrogen-containing molecules, N=1 likely refers to deprotonated species, while N=2 likely means that the molecule is charged by NO_3^-. When N=3, it is possible that the molecule is charged by nitric acid dimer, $HNO_3{\cdot}NO_3^-$, or has two nitrogens within a molecule and is charged by NO_3^-. m/z is mass-to-charge ratio and f_{total} is fraction of total signal.

Non-nitrogen containing HOM								
C	**H**	**O**	**N**	**m/z, Th**	**f_{total}x10^{-6} panel a**	**f_{total}x10^{-6} panel b**	**f_{total}x10^{-6} panel c**	**f_{total}x10^{-6} panel d**
5	7	6	0	163.0248	8	61	13	29
6	5	6	0	173.0092	37	167	41	74
6	5	8	0	204.9990*	17	87	33	n/a
6	7	8	0	207.0146	11	55	43	25
6	5	9	0	220.9939*	14	39	44	n/a
5	4	9	1	221.9892	74	328	104	59
5	6	9	1	224.0048	47	230	43	46
6	4	9	1	233.9892	20	189	53	27
6	6	9	1	236.0048	103	429	360	142
6	7	9	1	237.0126	30	58	88	41
5	6	10	1	239.9997	177	449	122	167
5	7	10	1	241.0075	35	81	56	109
6	4	10	1	249.9841	19	302	41	51
6	6	10	1	251.9997	68	852	284	102
6	8	10	1	254.0154	130	857	236	98
5	5	11	1	254.9868	20	306	41	64
5	6	11	1	255.9946	1135	585	93	403
6	4	11	1	265.9790	22	175	45	62
6	5	11	1	266.9868*	51	44	68	n/a
6	6	11	1	267.9946	107	901	144	154
6	7	11	1	269.0025	42	271	80	67
6	8	11	1	270.0103	363	984	285	201
6	6	12	1	283.9895	124	577	220	607
6	7	12	1	284.9974*	153	215	66	132
6	8	12	1	286.0052	265	749	442	171
6	9	12	1	287.0130*	58	187	67	n/a
6	10	12	1	288.0208	55	297	69	n/a
5	8	13	1	290.0001	39	107	25	31
6	6	13	1	299.9845	277	342	140	123
6	8	13	1	302.0001	718	474	393	190
5	7	14	1	304.9872	31	85	45	41
5	8	14	1	305.9950	28	65	28	19
6	8	14	1	317.9950	374	251	83	111
6	9	14	1	319.0029*	292	210	36	n/a
6	10	14	1	320.0107	78	73	241	62
10	8	12	1	334.0052	110	180	81	55

Table S4. Continued.

C	H	O	N	m/z, Th	$f_{total}x10^{-6}$ panel a	$f_{total}x10^{-6}$ panel b	$f_{total}x10^{-6}$ panel c	$f_{total}x10^{-6}$ panel d
10	9	12	1	335.0130	61	206	31	50
10	10	12	1	336.0208	62	141	107	35
12	12	11	1	346.0416*	58	40	144	n/a
12	14	11	1	348.0572	309	62	78	58
11	14	12	1	352.0521	103	61	119	22
10	12	13	1	354.0314	47	45	93	18
12	12	12	1	362.0365*	120	60	264	n/a
12	14	12	1	364.0521	147	70	170	64
12	16	12	1	366.0678	53	53	48	23
11	14	13	1	368.0471	44	63	68	18
10	12	14	1	370.0263	27	50	42	18
12	12	13	1	378.0314	90	95	316	53
12	14	13	1	380.0471	143	119	178	33
12	16	13	1	382.0627	58	68	49	22
11	14	14	1	384.0420	52	62	53	19
10	12	15	1	386.0212	34	50	30	24
12	10	14	1	392.0107	15	25	33	14
12	12	14	1	394.0263*	71	90	269	n/a
12	14	14	1	396.0420	115	134	132	34
12	16	14	1	398.0576	97	124	62	23
11	14	15	1	400.0369	40	50	20	16
12	10	15	1	408.0056	8	29	23	13
12	12	15	1	410.0212	149	95	297	34
12	14	15	1	412.0369	166	123	78	27
11	12	16	1	414.0162	51	81	29	17
11	14	16	1	416.0318	34	46	6	14
12	10	16	1	424.0005	11	28	25	12
12	12	16	1	426.0162*	95	70	90	n/a
12	14	16	1	428.0318	126	108	102	29
12	16	16	1	430.0475	36	66	18	15
11	14	17	1	432.0267	32	38	13	7
12	12	17	1	442.0111	36	54	42	15
12	14	17	1	444.0267	338	81	51	20
12	16	17	1	446.0424	34	46	16	16
12	12	18	1	458.0060	21	38	24	8
12	14	18	1	460.0216	44	48	23	13
12	16	18	1	462.0373	24	30	28	7
12	12	19	1	474.0009	10	20	4	3
12	14	19	1	476.0166	31	27	21	9
12	16	19	1	478.0322	16	18	25	7
12	16	20	1	494.0271	11	14	13	2
12	14	21	1	508.0064	9	8	10	3
12	16	21	1	510.0220	4	9	7	4

Table S4. Continued.

Nitrogen-containing molecules						
C	**H**	**O**	**N**	**m/z, Th**	**$f_{total}x10^{-6}$ panel d**	**Likely compound**
6	4	3	1	138.0196666	101.6	deprotonated nitrophenol
6	4	4	1	154.0145812	352.7	depritonated nitrocatechol
6	5	6	2	201.0153095	673.1	nitrophenol with NO_3^-
5	5	7	2	205.0102241	50.1	
6	5	7	2	217.0102241	307.1	nitrocatechol with NO_3^-
5	5	8	2	221.0051387	49.2	
3	5	10	2	228.9949679	22.9	
6	7	8	2	235.0207888	326.3	
6	5	9	2	249.0000533	178.4	
6	6	9	3	264.0109524	1217.1	likely nitrophenol with $HNO_3^-NO_3^-$
6	7	10	2	267.010618	82.3	
5	7	11	2	271.0055326	55.8	
4	5	12	2	272.9847972	62.7	
4	7	12	2	275.0004472	31.5	
6	6	10	3	280.005867	140.3	nitrocatechol with $HNO_3^-NO_3^-$
6	5	11	2	280.9898826	71.3	
6	7	11	2	283.0055326	133.3	
5	7	12	2	287.0004472	74.0	
4	6	12	3	287.9956962	49.2	
6	5	12	2	296.9847972	50.3	
6	7	12	2	299.0004472	154.2	
5	5	13	2	300.9797118	n/a	
6	9	12	2	301.0160973	136.1	
5	7	13	2	302.9953619	100.2	
4	6	13	3	303.9906108	74.3	
6	8	12	3	314.0113463	67.8	
6	7	13	2	314.9953619	148.9	
5	7	14	2	318.9902765	117.8	
6	6	13	3	327.9906108	60.3	
6	5	14	2	328.9746264	40.4	
6	8	13	3	330.0062609	77.6	
6	7	14	2	330.9902765	195.2	
6	9	14	2	333.0059266	90.1	
6	4	14	3	341.9698754	36.8	
6	8	14	3	346.0011755	98.7	
6	7	15	2	346.9851911	171.0	
6	9	15	2	349.0008412	51.0	
6	8	15	3	361.9960901	85.0	
6	7	16	2	362.9801057	75.1	
6	8	17	3	393.9859194	71.5	
6	8	19	3	425.9757486	24.8	